AD-A065 836 BELL AEROSPACE TEXTRON BUFFALO N Y F/G 20/4
NUMERICAL MODEL DEVELOPMENT FOR LASER CAVITY FLOWFIELDS.(U)
MAY 78 J T SCHIMKE, W L RUSHMORE, S W ZELAZNY F49620-77-C-0076
UNCLASSIFIED 9278-950001 AFOSR-TR-79-0085 NL

| OF |
AD
A065836

END
DATE
FILMED
5-79
DDC

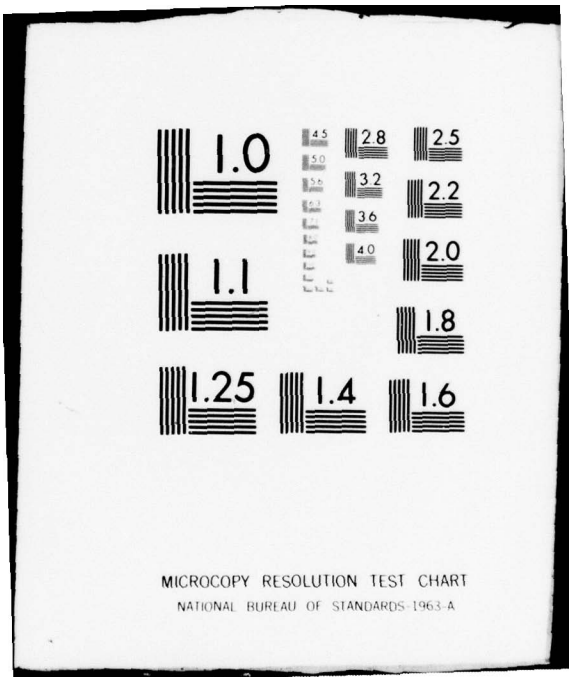
1.0
1.1
1.25
1.4
1.6
1.8
2.0
2.2
2.5
2.8
3.2
3.6
4.0
4.5
5.0
5.6
MICROCOPY RESOLUTION TEST CHART
NATIONAL BUREAU OF STANDARDS-1963-A

NUMERICAL MODEL DEVELOPMENT FOR LASER CAVITY FLOWFIELDS

FOR PERIOD COVERING MAY 31, 1977 TO MAY 31, 1978

J. T. SCHIMKE
W. L. RUSHMORE
S. W. ZELAZNY

FOR

DEPARTMENT OF THE AIR FORCE
AIR FORCE OFFICE OF SCIENTIFIC RESEARCH (AFSC)
BOLLING AIR FORCE BASE, DC 20332

NUMERICAL MODEL DEVELOPMENT
FOR
LASER CAVITY FLOWFIELDS

FOR PERIOD COVERING MAY 31, 1977 TO MAY 31, 1978

J. T. SCHIMKE
W. L. RUSHMORE
S. W. ZELAZNY

FOR

DEPARTMENT OF THE AIR FORCE
AIR FORCE OFFICE OF SCIENTIFIC RESEARCH (AFSC)
BOLLING AIR FORCE BASE, DC 20332

SUMMARY

This report describes the results of the first year's efforts on AFOSR Contract F49620-77-C-0076, Numerical Model Development for Laser Cavity Flow Fields and covers the period May 31, 1977 to May 31, 1978. Two specific types of numerical models are considered in this investigation, i.e., models for quasi two-dimensional unsteady flows and three-dimensional steady mixing and reacting flow fields. Earlier investigations at Bell Aerospace Textron led to the development of a three-dimensional (3D) flow model which was restricted to constant area single specie flow problems. Also this model used an explicit integration scheme which resulted in relatively long computer solution times. During the past year, the 3D flow model was extended to consider multispecie diffusional flow fields in laser cavities of variable cross section. Also an implicit integration algorithm was used to replace the explicit integration scheme resulting in computer solution times in excess of a factor of five faster than the explicit integration technique. The resulting model was applied to a three-dimensional laser cavity mixing problem to predict the magnitude of mixing and reacting induced density (and index of refraction) striations. Results show that for the low pressure cavity conditions of interest variation media density induced by nonuniform mixing will be small, e.g., optical path differences of less than one fifteenth of a hydrogen fluoride laser wavelength.

In addition to using implicit integration methods in the 3D steady state study, these methods were also employed in our investigation of unsteady flow modeling techniques. Specifically, the GEARIB integration method was used in conjunction with the box method of spatial discretization on a variety of one-dimensional unsteady gas flow problems. The test case problems used to establish the accuracy and sensitivity of the unsteady model to boundary conditions and discretization parameters included: (1) steady state gas flow in variable area ducts, (2) hyperbolic unsteady flows (streamwise diffusion neglected), and (3) parabolic unsteady flows (streamwise diffusion considered). Unsteady flows with heat addition were also analyzed with various upstream and downstream boundary conditions to characterize various types of detonation and deflagration conditions. Many of the numerical difficulties encountered in the solution of these problems are also expected to be present in the unsteady laser flows which are being examined during the second year of this investigation.

Section I of this report describes the coordinate transformation used in the three-dimensional flow model. Implicit integration methods are discussed in Section II where the advantages and disadvantages of these methods are reviewed. Numerical results for a variety of nonlinear parabolic (2D and 3D) problems solved using both finite element and finite difference techniques are given in Section III. Two simple unsteady flow problems which were used in the initial check out phases of our unsteady model development are described in Section IV followed by a description of the results of analyses of a number of unsteady flow problems in Section V. Recommendations are given in Section VI.

TABLE OF CONTENTS

LIST OF ILLUSTRATIONS

TABLES

I. THREE-DIMENSIONAL FLOW MODEL COORDINATE TRANSFORMATION

A. Introduction

In the original version of the parabolic Navier-Stokes variant of the COMOC computer program, it was assumed that the cross-sectional area of the flow region (duct) remained constant with the streamwise coordinate. It is possible to relax this restriction. The generalized equations for certain types of cross-section variation have been derived and built into the COMOC program and have been checked out for some simple cases.

B. Details of the Coordinate Transformation

By an appropriate transformation of variables (essentially coordinate stretching), the cross section in the (y,z) plane may be allowed to grow as a specified function of the mass flow coordinate x, Figure 1.1. This is essential in computing confined flows in variable area ducts (i.e., laser cavities). The finite element grid is established at the initial cross-sectional geometry and then the finite elements in the cross section expand or contract as the flow moves downstream.

The coordinate transform is defined as follows: Consider a flow bounded in the y direction by walls of a specified geometry $y = f_1(x)$ and $y = f_2(x)$, and also bounded in the z direction by walls $z = g_1(x)$ and $z = g_2(x)$ (see Figure 1.1).

The transformation from (x,y,z) coordinates to (ξ,η,ζ) coordinates is given by:

$$\xi = x$$

$$\eta = \frac{y - f_1(x)}{f_2(x) - f_1(x)} \tag{1.1}$$

$$\zeta = \frac{z - g_1(x)}{g_2(x) - g_1(x)}$$

This transform maps any variable cross section in the (y,z) plane to a rectangular cross section in the η,ζ plane given by (see Figure 1.1):

$$0 \leq \eta \leq 1$$

$$0 \leq \zeta \leq 1 \tag{1.2}$$

Of interest is the species continuity equation for the mass fraction Y_i of each specie in the transformed coordinates. The governing species continuity equation in (x,y,z) coordinates is given by:

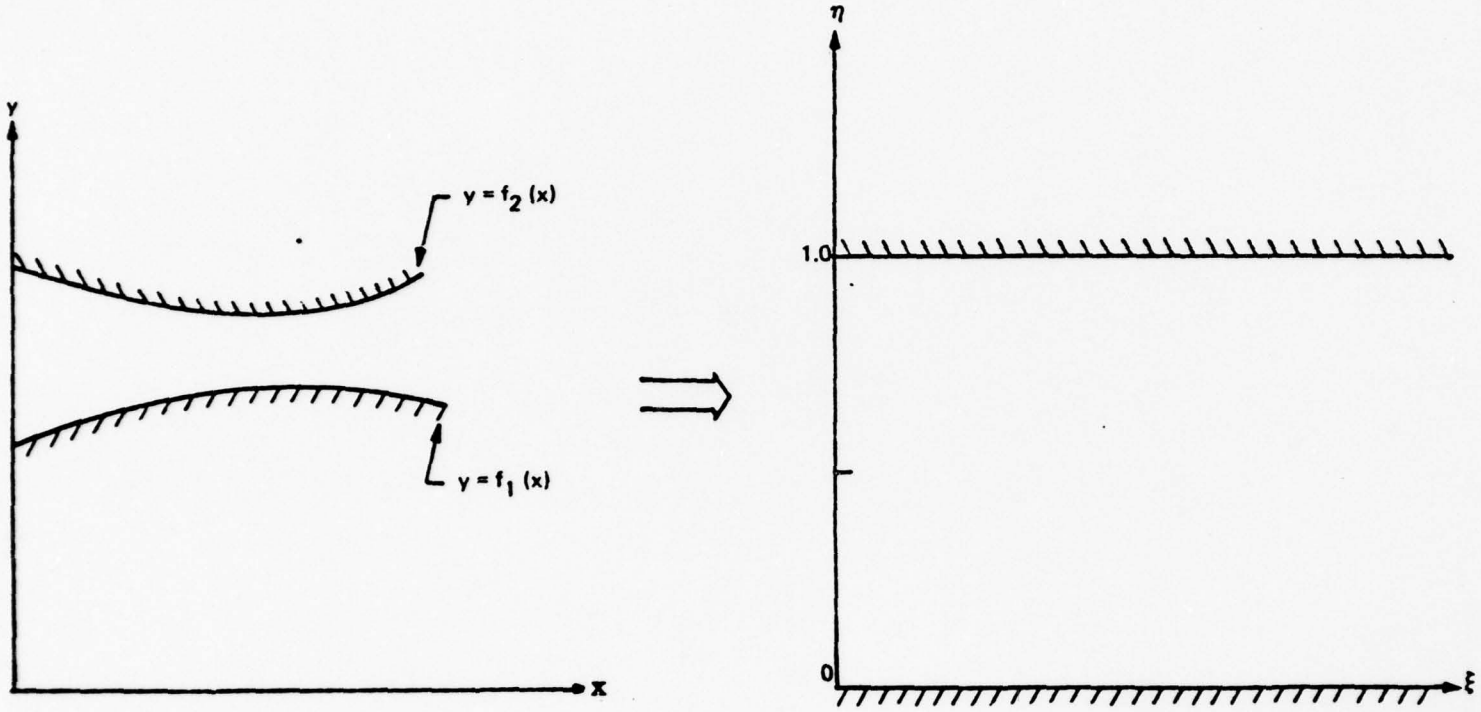

Figure 1.1. Variable Geometry Transformation in the y Direction

$$\rho u \frac{\partial Y_i}{\partial x} + \rho v \frac{\partial Y_i}{\partial y} + \rho w \frac{\partial Y_i}{\partial z}$$

$$= \frac{\partial}{\partial y}\left(\frac{\mu^e}{N^e_{Sc}\, N_{Re}} \frac{\partial Y_i}{\partial y}\right) + \frac{\partial}{\partial z}\left(\frac{\mu^e}{N^e_{Sc}\, N_{Re}} \frac{\partial Y_i}{\partial z}\right) + S_i \qquad (1.3)$$

The variables appearing in equation (1.3) are non-dimensionalized with respect to U_∞, ρ_∞, μ_∞ and a length scale L. The Reynolds number N_{Re} is given by:

$$N_{Re} = \frac{U_\infty \rho_\infty L}{\mu_\infty} \qquad (1.4)$$

The effective Prandtl number N^e_{Pr} and Schmidt number N^e_{Sc} are defined for a combination of laminar and turbulent contributions as:

$$\frac{\mu^e}{N^e_{Pr}} = \frac{\mu}{N_{Pr}} + \frac{\rho\varepsilon}{(N_{Pr})_T} \qquad (1.5)$$

$$\frac{\mu^e}{N^e_{Sc}} = \frac{\mu}{N_{Sc}} + \frac{\rho\varepsilon}{(N_{Sc})_T}$$

In equation (1.5), μ is the laminar viscosity, ε is the kinematic eddy (effective) viscosity, and the subscript T denotes a turbulent parameter.

Using the coordinate transformation given by equation (1.1), the species continuity equation in the transformed coordinates becomes:

$$\rho u \frac{\partial Y_i}{\partial \xi} + F_1 \rho v \frac{\partial Y_i}{\partial \eta} + G_1 \rho w \frac{\partial Y_i}{\partial \zeta}$$

$$= \rho u\left[(F_2 + \eta F_3) \frac{\partial Y_i}{\partial \eta} + (G_2 + \zeta G_3) \frac{\partial Y_i}{\partial \zeta}\right] \qquad (1.6)$$

$$+ F_1^2 \frac{\partial}{\partial \eta}\left(\frac{\mu^e}{N^e_{Sc}\, N_{Re}} \frac{\partial Y_i}{\partial \eta}\right) + F_2^2 \frac{\partial}{\partial \zeta}\left(\frac{\mu^e}{N^e_{Sc}\, N_{Re}} \frac{\partial Y_i}{\partial \zeta}\right) + S_i$$

where

$$F_1(\xi) = \frac{1}{f_2(\xi) - f_1(\xi)} \qquad G_1(\xi) = \frac{1}{g_2(\xi) - g_1(\xi)}$$

$$F_2(\xi) = \frac{f_1'(\xi)}{f_2(\xi) - f_1(\xi)} \qquad G_2(\xi) = \frac{g_1'(\xi)}{g_2(\xi) - g_1(\xi)} \tag{1.7}$$

$$F_3(\xi) = \frac{f_2'(\xi) - f_1'(\xi)}{f_2(\xi) - f_1(\xi)} \qquad G_3(\xi) = \frac{g_2'(\xi) - g_1'(\xi)}{g_2(\xi) - g_1(\xi)}$$

and the primes denote differentiation with respect to ξ.

The transformation given by equation (1.6) has been incorporated into COMOC and checked out for a simple geometry.

II. IMPLICIT INTEGRATION METHODS

A. Introduction

One of the principal objectives of this study is to examine the advantages of implicit methods for integrating large systems of ordinary differential equations arising from the spatial discretization (by finite differences or finite elements) of the partial differential equations governing two major classes of fluid dynamics problems:

i) steady boundary layer and parabolic Navier-Stokes problems in two and three dimensions (3D)

ii) unsteady gas flow in one dimension

B. Advantages and Disadvantages of Implicit Integration Methods

At Bell Aerospace Textron problems of type (i) have been solved for a number of years using the COMOC continuum mechanics program (Baker and Zelazny [1]) which employs triangular finite elements for the spatial discretization, and uses an explicit method with an extended region of absolute stability for the integration of the resulting ordinary differential system. (This integration is performed in the direction of the streamwise coordinate, which has a time-like character.) See Nigro [2] for the development of this explicit method. In spite of the improved stability of this method (in comparison to conventional explicit methods), the inherent stiffness of the differential systems arising in many applications (especially when strong diffusive effects are present) severely restricts the step-size of such explicit methods. This is to say nothing of problems involving finite rate chemistry which must be tackled in future 3D laser simulations at Bell. The high chemical reaction rates make such problems several orders of magnitude stiffer than those involving only diffusive processes. Consequently, it is imperative that explicit methods be replaced by implicit methods, which have far better absolute stability properties.

For the second class of problems (ii) it is traditional to use explicit integration methods since the partial differential system for many applications is hyperbolic (i.e., there are no diffusive effects), which means that the ordinary differential system resulting from spatial discretization is not stiff and can be solved efficiently by explicit techniques. However, if diffusive effects (e.g., viscosity, heat conduction) and/or finite rate chemistry are present, the resulting ordinary differential system is stiff, and explicit methods are no longer appropriate. Examples of such problems involving viscosity and heat conduction are given later in this report.

In addition to their improved absolute stability properties, there is a further advantage in going to implicit methods. Consider the following general form of the system of ordinary differential equations (ODE's) arising from the spatial discretization of the system of partial differential equations (PDE's) under consideration:

$$\begin{bmatrix} & & \\ & A(t,y_1,y_2,\ldots,y_N) & \\ & & \end{bmatrix} \begin{Bmatrix} \dot{y}_1 \\ \dot{y}_2 \\ \cdot \\ \cdot \\ \cdot \\ \cdot \\ \cdot \\ \dot{y}_N \end{Bmatrix} = \begin{Bmatrix} f_1(t,y_1,y_2,\ldots,y_N) \\ f_2(t,y_1,y_2,\ldots,y_N) \\ \cdot \\ \cdot \\ \cdot \\ \cdot \\ \cdot \\ f_N(t,y_1,y_2,\ldots,y_N) \end{Bmatrix} \tag{2.1}$$

Here the "dot" denotes the time derivative (or, in the case of boundary layer and parabolic Navier-Stokes problems, the derivative in the direction of the spatial coordinate having time-like character). A is an N by N matrix, which may depend on t and the dependent variables, y_i (but not on $\dot{y}_i$). Note that A is not required to be non-singular. (In fact, the A-matrix is singular for a number of examples discussed later in this report.) Now in order to use an explicit method to integrate (2.1), it is first necessary to solve for the derivative vector. If A is singular, it will be difficult or impossible to do this. For A non-singular this requires the solution of an Nth order matrix equation. (For the purposes of this report, the solution of a matrix equation will be thought of as a factorization of the A-matrix followed by a back substitution based on the factors of A and the particular RHS vector.) Excluding the special case where A is constant and can therefore be factored once and for all, it is necessary to re-factor A every time a fresh derivative evaluation is required by the particular explicit method. This factorization is an expensive process unless A is of some special form which allows for very efficient factorization. Of course, the preferred form is a diagonal A, and most spatial differencing schemes used in conjunction with explicit methods yield a diagonal A-matrix. This requirement of a diagonal A-matrix is a restriction which makes it more difficult to obtain high order accuracy in the spatial discretization, especially for non-uniform meshes. For example, with finite element discretizations, the A-matrix is naturally non-diagonal. To obtain a diagonal matrix multiplying the derivative vector, a process popularly known as "lumping" has often been used. Lumping consists of replacing the A-matrix with a diagonal matrix, each element of which is the sum of the elements in the corresponding row of the A-matrix. For the simplest elements having linear shape functions, this procedure alters the approximate solution somewhat but does not lower the order of the approximation. (The COMOC program, which uses linear shape functions over triangular elements, employs lumping so that the explicit method mentioned previously can be used.) However, for higher order elements lumping reduces the order of accuracy and should not be used. See Strang and Fix [3] for a discussion of lumping.

If it is decided to use a spatial differencing scheme yielding a non-diagonal A-matrix, then an explicit method will require the same order of magnitude of computation per step (principally the time consuming factorization of A) as an implicit method, and so, inrespective of any stability considerations, there is no advantage in using an explicit method. In fact, the implicit methods that are used in this study, Hindmarsh [4], do not require a refactorization of the A-matrix at every step, and therefore require even less computation per step (on an average) than explicit methods.

C. Implicit Integration Method Used in the Study

There are a number of implicit integration methods with good absolute stability properties which could be selected. The best known of these are the backward Euler method, the trapezoidal method, and the method of Curtiss and Hirschfelder [5]. The backward Euler is a first order method while the other two are second order. Instead of selecting only one such method, a better strategy would be to use a family of implicit methods, each one being of different order, and using the particular member of the family that would allow the largest possible step consistent with the accuracy requirements for the problem being treated. Fortunately, subroutine packages which do exactly this are readily available. The first widely available package of this sort is due to Gear [6]. (Two of the methods in this package are the backward Euler and that of Curtiss and Hirschfelder.) Later other packages, all based on the methods of Gear were developed at the Lawrence Radiation Laboratory by Hindmarsh and his colleagues. The particular package used in this study is known as GEARIB [4]. It is designed to treat ordinary differential systems for which the A-matrix is non-diagonal, banded, and possibly even singular. Like all the packages based on that of Gear, GEARIB automatically varies the integration step size and order so that the integration can be carried out as efficiently as possible subject to the user supplied accuracy requirement.

When using implicit methods for ordinary differential systems which are nonlinear (the case for practically all of the examples of this report), it is necessary to solve a large system (of size N, the number of dependent variables) of nonlinear algebraic equations at each step. This is not as bad as it seems, since a good starting guess for the solution of these nonlinear equations is available from the prediction (using an explicit predictor) from the preceding step. Usually, only one or two iterations using Newton's method are required to home in on the solution. The apparent drawback is that for Newton's method the N by N Jacobian matrix of the nonlinear algebraic system must be formed and factored for each iteration. However, since the dependent variables of the problem change smoothly (usually) the elements of this Jacobian do not change rapidly and it is usually unnecessary to form and factor this Jacobian for every iteration. In fact GEARIB is set up to re-evaluate and factor the Jacobian only when the iterative solution to the nonlinear system is converging too slowly. Typically, this is every 10 integration steps or so. The convergence of this modified Newton's method (sometimes referred to as a quasi-Newton method) is somewhat slower than the true Newton method. However, the great reduction in Jacobian formations and factorizations more than compensates for the lower convergence rate.

III. THE COMOC PROGRAM: BOUNDARY LAYER AND PARABOLIC NAVIER-STOKES PROBLEMS

A. Introduction

In this section, numerical results for a variety of nonlinear parabolic problems solved by:

i) COMOC with the original explicit integration method

ii) COMOC with the new implicit integration method (GEARIB)

are compared, especially with regard to efficiency.

B. Blasius Boundary Layer by Finite Differences

Before using GEARIB in conjunction with the finite element spatial discretization (COMOC) of the Blasius boundary layer equations, it was decided to test GEARIB with a more conventional finite difference spatial discretization of these equations. These solutions will be useful for later comparison with the corresponding COMOC results.

The Blasius equations for incompressible boundary layer flow are:

$$\frac{\partial u}{\partial x} = -\frac{\partial v}{\partial y} \tag{3.1a}$$

$$u\frac{\partial u}{\partial x} = -v\frac{\partial u}{\partial y} + \frac{\partial^2 u}{\partial y^2} - \frac{dp}{dx} \tag{3.1b}$$

Here x and y are the streamwise and transverse coordinates, respectively, and u and v are the corresponding velocity components. dp/dx is the prescribed pressure gradient. Upon discretizing (3.1) in the transverse direction by finite differences, the following differential system results:

$$\begin{bmatrix} 0 & .5 & 0 & 0 & 0 & 0 & \cdots \\ 0 & u_1 & 0 & 0 & 0 & 0 & \\ 0 & .5 & 0 & .5 & 0 & 0 & \\ 0 & 0 & 0 & u_2 & 0 & 0 & \\ 0 & 0 & 0 & .5 & 0 & .5 & \\ 0 & 0 & 0 & 0 & 0 & u_3 & \\ \vdots & & & & & & \end{bmatrix} \begin{Bmatrix} \dot{v}_1 \\ \dot{u}_1 \\ \dot{v}_2 \\ \dot{u}_2 \\ \dot{v}_3 \\ \dot{u}_3 \\ \vdots \end{Bmatrix} = \begin{Bmatrix} -v_1/H \\ -v_1u_2/2H + (u_2 - 2u_1)/H^2 - dp/dx \\ -(v_2 - v_1)/H \\ -v_2(u_3 - u_1)/2H + (u_3 - 2u_2 + u_1)/H^2 - dp/dx \\ -(v_3 - v_2)/H \\ -v_3(u_4 - u_2)/2H + (u_4 - 2u_3 + u_2)/H^2 - dp/dx \\ \vdots \end{Bmatrix} \tag{3.2}$$

Here the dots above the u_i and v_i on the left denote derivatives with regard to x. H is the uniform mesh size. The mesh starts at the wall with mesh point 0. However, since u_o and v_o vanish on the wall they do not appear in (3.1). The even numbered rows correspond to the second order finite difference representation of (3.1b) written at the mesh points. The odd numbered rows represent the continuity equation (3.1a) written at the center of each mesh interval to second order accuracy. The last mesh point, y_N, is chosen to lie well into the free stream where the velocity u_N is known; for the Blasius problem $u_N = 1$. v_N is unknown. Thus, there are (N-1) values of u_i and N values of v_i to be determined at each integration step making (2N-1) unknowns altogether. Because (3.1a) was written at the center of each mesh interval and (3.1b) at each interior mesh point, there are also (2N-1) equations in system (3.2).

Note that (3.2) is not in normal form. It cannot even be put in normal form, the odd columns are zero. This was no impediment to the implicit integration package, GEARIB. It integrated (3.2) as it stands completely satisfactorily. Various test runs were made using anywhere from 12 to 50 mesh points over the y-interval [0,1]. The numerical solutions were compared to the "exact" solution presented in Schlichting [7], p. 120 ff. The error behaved as expected with the different mesh sizes. (Practically all the error was due to the finite difference discretization in the y-direction. The error per step criterion, ε, for GEARIB was chosen to be 10^{-4} or 10^{-5}, which meant that the integration of system (3.2) was quite accurate.) Equation (3.2) was generalized to unequal mesh sizes and by a judicious mesh selection (about three times as fine near y = 0 relative to y = 1) further improvements were obtained for a given number of mesh points. It is interesting that the errors in the v_i were generally an order of magnitude greater than those for the u_i. This condition continued to be true for the finite element solutions discussed in the next subsection.

For the numerical tests, dp/dx was set to zero in (3.2) consistent with the Blasius problem. However, a non-zero pressure gradient would introduce no additional complication. The integration began at x = 1 and continued to x = 2. By x = 2, the boundary layer had grown enough that further integration would have meant nonuniform conditions would be obtained near y = 1, inconsistent with the boundary layer assumptions. Integration beyond x = 2 would have required a mesh extending over a larger range of y.

To obtain initial values for u_i, the tabulated "exact" solution of Schlichting was fitted with a cubic spline, which was then used to obtain interpolated values at the points of our finite difference mesh. The same thing was done for the v_i. However, these initial values for the v_i were less satisfactory (from the standpoint of starting the integration) than those obtained by the following method: Referring to (5.2), it can be seen that there are two equations for $\dot{u}_1$, two for $\dot{u}_2$, etc. Having selected the u_i, the v_i should be selected so that these pairs of equations are consistent. It is a simple matter to set up equations corresponding to this requirement. These equations are almost trivially solved for the v_i in succession. With the u_i and v_i so chosen, it would be possible to solve for the initial $\dot{u}_i$, which could be useful for the initial prediction by GEARIB. However, for simplicity the initial $\dot{u}_i$ and v_i were set to zero. The integration got started satisfactorily inspite of the poor prediction based on these arbitrarily chosen derivatives.

C. Blasius Boundary Layer by Finite Elements

The boundary layer option in the COMOC computer program has been designed for three-dimensional boundary problems. Transverse planes normal to the direction of the main flow are subdivided into triangular elements. The variables of the problem are expressed in terms of the nodal values of these variables assuming a linear variation of the particular variable over the triangular element. Thus, a two-dimensional problem must be solved as a three-dimensional problem if COMOC is to be used. In doing this the simplest possible finite element grid is used which is illustrated in Figure 3.1. To preserve the two-dimensionality of the

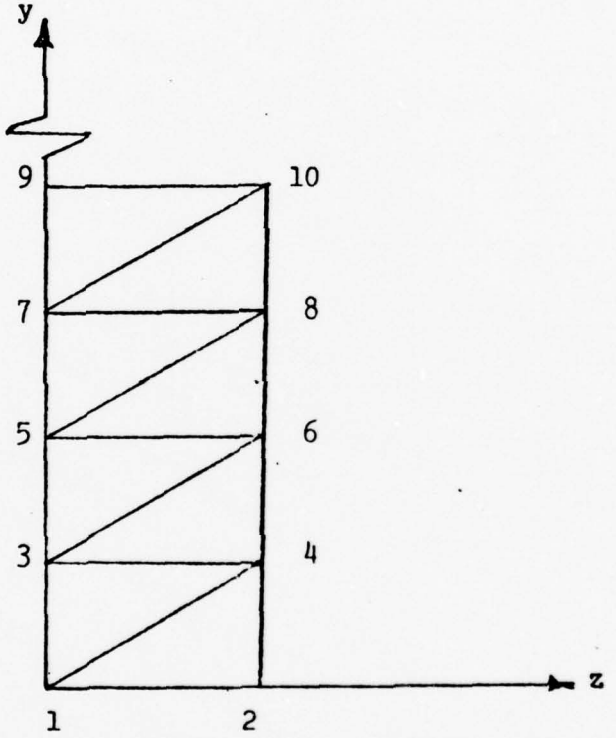

Figure 3.1 Finite Element Discretization for Two-Dimensional Problems

problem, zero gradient boundary conditions are imposed on the z = constant faces of this grid. The boundary conditions on the y = constant faces are the same as in the finite difference case. Because this finite element grid requires two columns of nodes, there will be twice as many problem unknowns, u_i and v_i, as for finite differences for the same fineness of discretization.

Before discussing numerical results from COMOC, one other significant difference between the finite difference approach shown in equation (5.2) and the finite element approach of COMOC should be noted. In COMOC, when solving the system of PDE's (3.1), only the discretized forms of the x-momentum equation are regarded as ordinary differential equations to be solved by marching methods. The discretized forms of the continuity equation are considered to be algebraic constraints to

which the marching integration must be subjected. (No such distinction is made between momentum and continuity in the finite difference formulation (5.2).)

The COMOC solution process goes as follows: For given initial conditions on u_i and v_i, the discretized forms of the x-momentum equation are advanced one step by the explicit integration method built into COMOC. If this step is deemed successful by the internal error control mechanism, then v_i is updated based on the finite difference equation,

$$v_{i+1} - v_i = -\frac{H_i}{2}\left(\frac{du_i}{dx} + \frac{du_{i+1}}{dx}\right) \tag{3.3}$$

where H_i is the y mesh spacing and du_i/dx is approximated by a finite difference formula involving the old and new values of u_i. Now $v_o = 0$, so (3.3) can be used to obtain the v_i in succession. After the v_i are so updated, the next step is begun.

Now this procedure for dealing with the continuity equation has been successful in many computations using COMOC. Initially our feeling was that this approach may be suitable when an explicit integration method is being used to advance the u_i. However, we were doubtful whether it would be appropriate when an implicit method, which often takes much larger integration steps, was being used. Nevertheless, for the first numerical work using COMOC modified to include GEARIB (instead of the old explicit method), it was decided to continue with this approach, but expecting to have to switch to a fully implicit treatment of continuity later.

For the basic Blasius test case, the finite element grid was based on 24 equally spaced intervals in the y-direction (see Figure 3.1). The initial conditions were chosen as in the finite difference solution. This problem was first solved with the unmodified COMOC (explicit integration). Although the problem was solved with an accuracy comparable to that of the finite difference approach, the CPU time to obtain this solution was rather large. The principal difficulty was that after the step size had built up to a certain point (after starting from a very small initial step), the error control mechanism in COMOC decided, based on the smoothness of the solution trajectories of the u_i, that a larger step size, h, could be used and still maintain the desired accuracy. Unfortunately, this error control mechanism has no means of reckoning with the conditional stability of the explicit method. The result was that after a few steps with this increased h, some of the rapid transients inherent in the differential system were spuriously excited because the step size fell outside the absolute stability limits of the explicit method. The error control mechanism then interpreted these growing transients as a legitimate part of the solution trajectories and cut back the step size in order to stay within the integration error bounds. After a few steps with this reduced h, the spurious transients would disappear. Again, the step size would be increased, and the whole cycle would get repeated. Although a good deal of CPU time was wasted with these erroneous step size changes, the CPU time would have been large even if the error

control mechanism had been able to keep the step size within the absolute stability limits of the explicit integration method. The reason is because this explicit method, despite its extended range of absolute stability, is still relatively restricted in its maximum step size.

On the other hand, when GEARIB replaced the explicit method in COMOC, the step size was limited only by accuracy requirements and not by stability considerations (since the GEARIB methods are implicit). In integrating from $x = 1$ to $x = 2$, the modified version of COMOC ran about five times as fast as the original version. This is somewhat misleading since the ratio of step sizes at $x = 2$ was about 40:1 in favor of the GEARIB version. If the integration had proceeded further, this ratio would have increased.

A variety of other discretization mesh sizes and integration accuracy criteria were tried. In all cases, the implicit method behaved as expected. However, in a number of these tests, the explicit method failed (usually by attempting step sizes too large for stability) and by the time this instability was detected it was too late to recover.

Despite the large integration step sizes possible with the implicit method, there was no evidence that the explicit treatment of the continuity equation in COMOC (discussed following equation (3.3)) resulted in any undesirable effects. However, there are some modifications of this explicit treatment that can result in modest increases in accuracy. One is that the updated value of $\dot{u}_i$ obtained in the course of an integration step by GEARIB can be used in formula (3.3) instead of a backward difference approximation to du_i/dx. This improves the accuracy somewhat at no additional expense. The other modification is that v_i can be updated from (3.3) after each prediction and correction by GEARIB, instead of just after a successful step. Again this results in better accuracy but at the expense of more CPU time (typically 25% more time).

Because the numerical results were satisfactory with this explicit treatment of the continuity equation, no attempt was made to modify COMOC for a fully implicit treatment of the governing equations (as was done in the previous section with the finite difference formulation). However, it would not be surprising to find that for more complicated boundary layer problems, e.g., three-dimensional, compressible, chemically reacting, such a fully implicit treatment would be desirable or even necessary. As discussed in the preceding subsection, GEARIB is designed to handle such implicit differential algebraic systems. COMOC could be modified to provide for fully implicit treatment of continuity, but at the expense of a significant amount of reprogramming.

D. Laser Cavity Mixing Demonstration Case

Striations in the laser cavity density field developing downstream of a laser nozzle array, Figure 3.2, have the potential of introducing optical path differences which will degrade laser beam quality, Gross and Bott [8]. Of specific interest is the region near the nozzle from the nozzle face to approximately four centimeters downstream. Here mixing and reaction is taking place between the cavity fuel

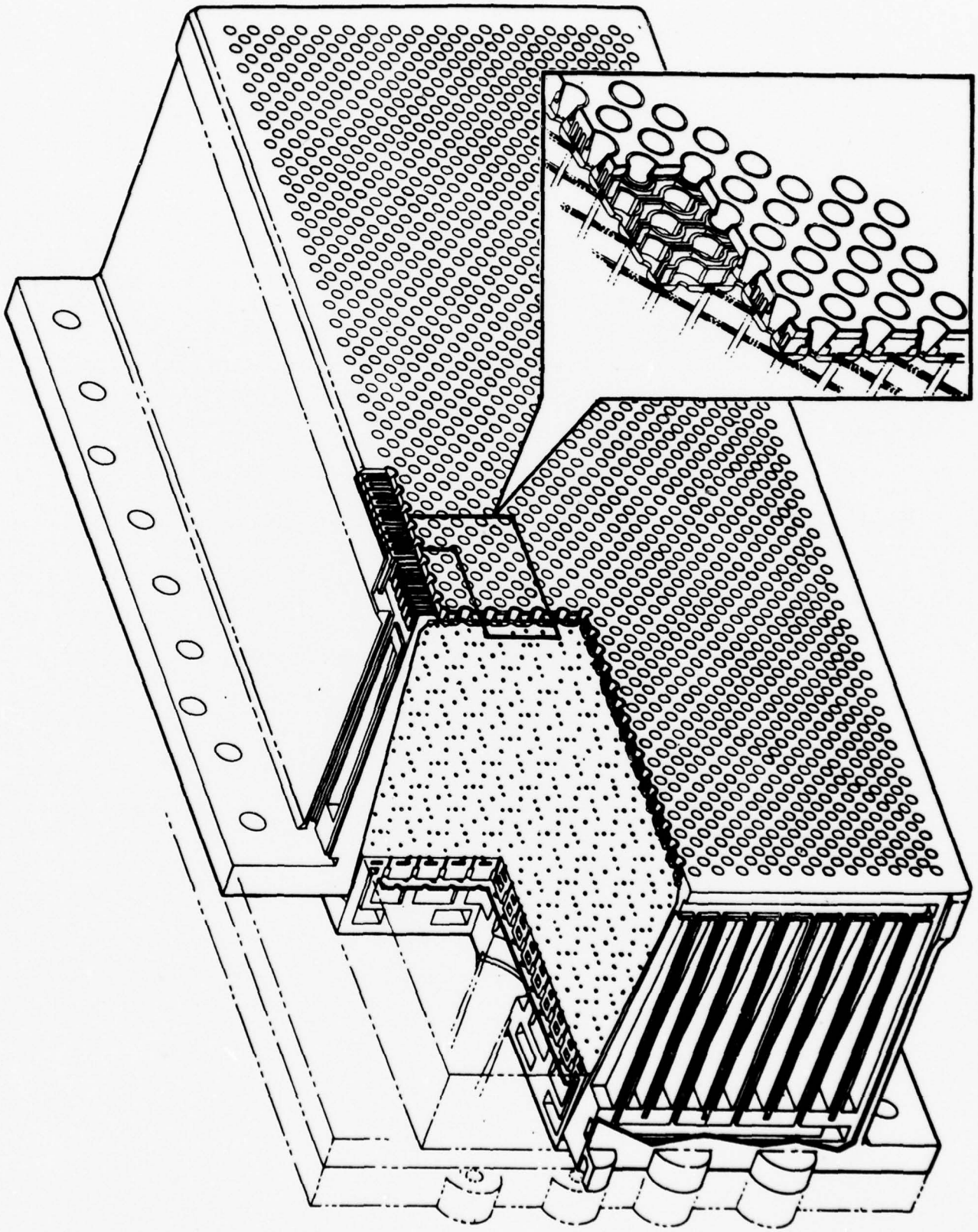

Figure 3.2 **Bell Aerospace Textron Three-Dimensional Axisymmetric Nozzle for Low Pressure Laser Cavity Applications**

(hydrogen) injected through the secondary (annular) nozzles and the oxidizer (fluorine) provided in the combustor and injected into the laser cavity by the primary nozzles. The starting conditions required at the nozzle exit/cavity entrance plane are obtained using the CNCDE code described by Driscoll [9]. Table 3.1 gives the velocities, temperatures, pressures, and mass fractions used in this demonstration case.

The change in optical path length is given by the expression

$$d\lambda = \rho(\beta/\rho_o)ds \tag{3.4}$$

where

$\beta \equiv$ Gladstone-Dale constant

$\rho_o \equiv$ the reference density at STP

$\rho \equiv$ local density

$ds =$ distance through the active media

$d\lambda =$ change in wave length due to variations in local density

Then

$$\Delta = \int_0^L \rho\left(\frac{\beta}{\rho_o}\right)_{mix} ds \tag{3.5}$$

Table 3.2 gives values of β/ρ_o for various gases of interest. The local value of β/ρ_o of a mixture is computed in terms of the local mass fractions Y_i using

$$\left(\frac{\beta}{\rho_o}\right)_{mix} = \sum_i Y_i \left(\frac{\beta}{\rho_o}\right)_i \tag{3.6}$$

Figure 3.3 shows a schematic of the computational domain analyzed and the finite element discretization field. The boundary conditions used in the computation required that mass, momentum, and energy diffusion across each boundary was zero. Seventy finite elements were used with forty-six node points and solution time on the IBM 360/65 computer was 2000 seconds for calculations over the range $0 < x < 3.08$ cm.

Applying equation (3.6) to the computed density field along three distinct paths produced the optical path differences shown in Figure 3.4. To be noted is that in all cases

Table 3.1 COMOC Starting Conditions

	Primary	Secondary
Velocity (ft/sec)	6380.	10660.
Temperature (°K)	468.	316.
Static Pressure (torr)	6.58	6.58
Y_i	0.339	0
Y_{DF}	0.518	0
Y_{He}	0.143	0
Y_{H_2}	0	1.0

Note: $Y_i \equiv$ mass fraction of specie i

Table 3.2 Gladstone Dale Constants

Specie	β/ρ_o (cm^3/gr)
F	0.01425
F_2	0.13409
He	0.21538
HF	0.16370
H_2	1.71077
N_2	0.26110

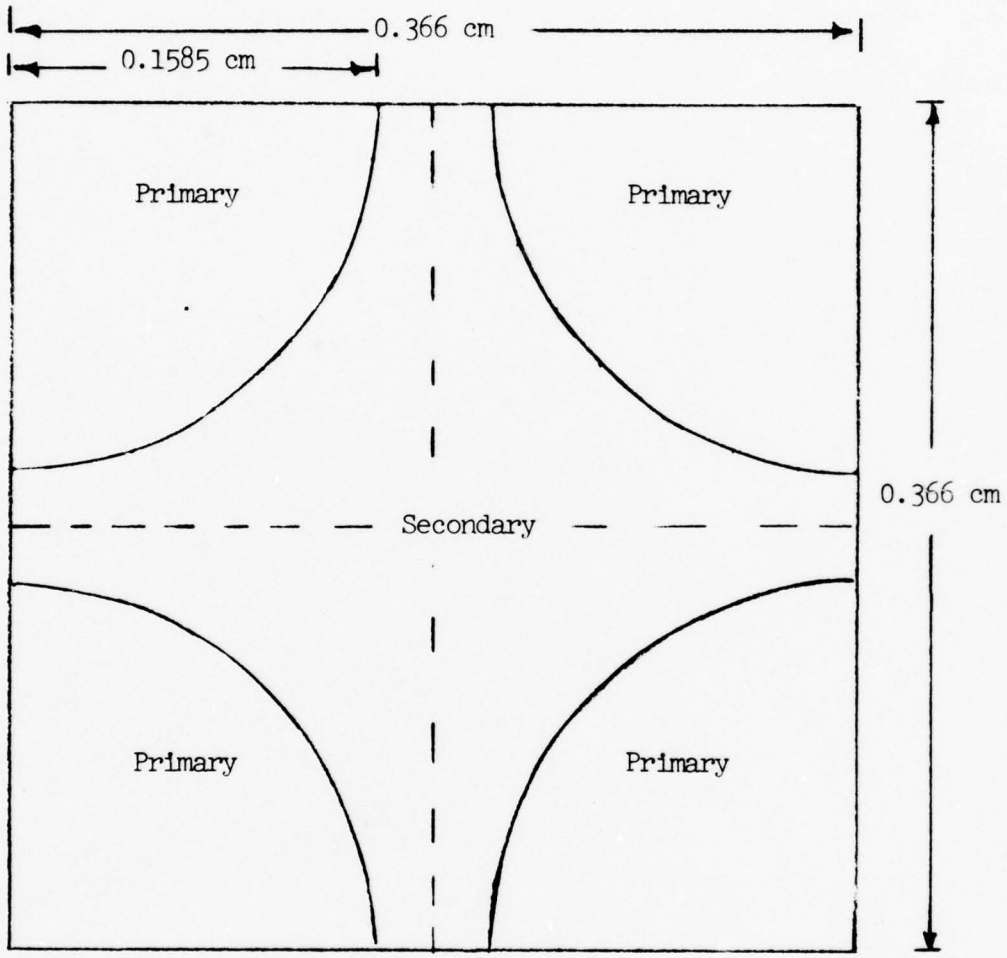

Figure 3.3(a) Computational Domain

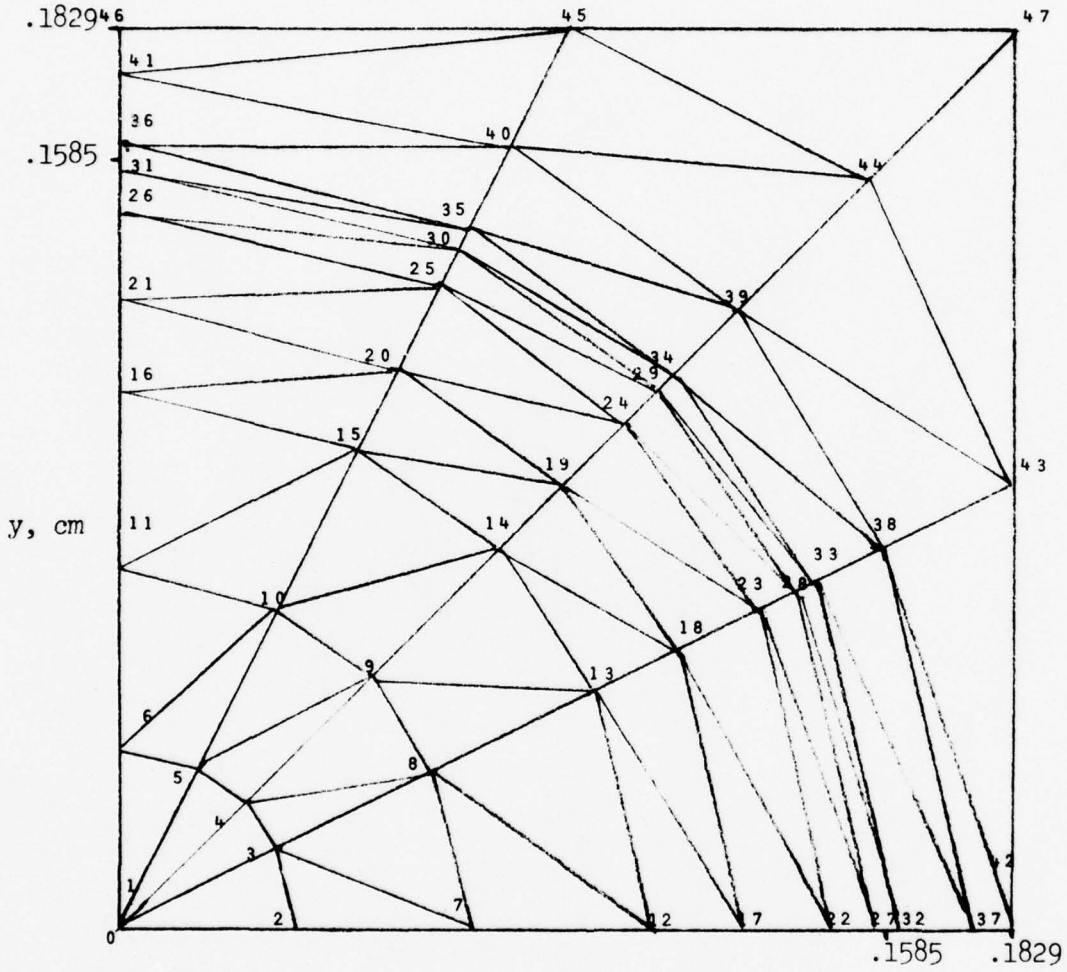

Figure 3.3(b) Finite Element Discretization

------- x = 0; Prior to Expansion
_____ · x = 1.0 cm; Region of Peak Gain
_____ x = 5.0 cm; Mixing Completed
_.-._.-. x = 5.0 cm; Mixing Completed

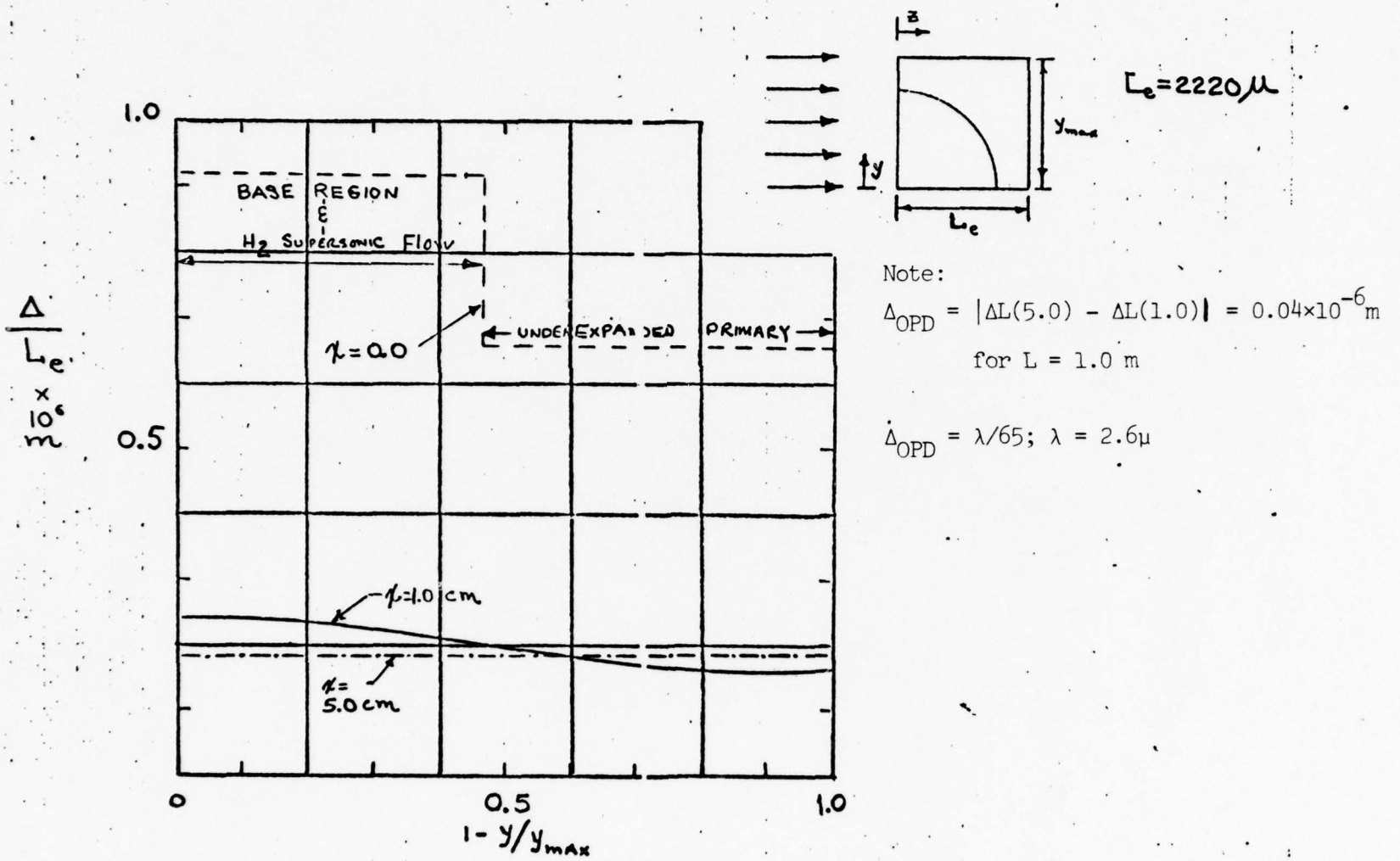

Note:

$\Delta_{OPD} = |\Delta L(5.0) - \Delta L(1.0)| = 0.04 \times 10^{-6}$ m

for L = 1.0 m

$\Delta_{OPD} = \lambda/65$; $\lambda = 2.6\mu$

Figure 3.4 Variation of Optical Path Length Across 3D mixing Zone

the maximum optical path difference which can be associated with striations induced by nonuniform mixing is less than $\lambda/50$. However, the variation in densities induced by variations in static pressure in both the lateral and longitudinal directions have the potential of inducing variations in optical path length in excess of $\lambda/50$. Lankford and Rapagnani [10] have observed transverse pressure variations in excess of a factor of two (17 torr to 34 torr) which exist downstream of the laser nozzle plane. Including this transverse pressure gradient influence in the three-dimensional model was beyond the scope of the current investigation.

IV. Simple One-Dimensional Unsteady Problems

A. Introduction

In this section two simple unsteady problems are discussed in detail and numerical results are presented. The first, coupled sound-heat flow, is linear and parabolic. The second, Burgers equation, is nonlinear and parabolic, although by appropriate specialization of the parameters of this partial differential equation, it can be reduced to the linear diffusion equation (parabolic) or a nonlinear traveling wave problem (hyperbolic). For some of these cases, there are exact solutions with which the numerical results can be compared. The spatial discretization used for these problems is carefully explained as is the application of GEARIB to solve the resulting ordinary differential systems.

B. Coupled Sound and Heat Flow

The first unsteady problem attempted was a linear parabolic problem, that of coupled sound and heat flow, which is discussed in detail on p. 264 f.f. of Richtmyer and Morton [11]. Further, there are exact solutions available (depending on initial and boundary conditions), which are convenient for assessing the accuracy of the numerical solution. After linearization, the governing partial differential equations are:

$$\frac{\partial e}{\partial t} = \sigma \frac{\partial^2 e}{\partial x^2} - c \frac{\partial u}{\partial x} \tag{4.1a}$$

$$\frac{\partial w}{\partial t} = c \frac{\partial u}{\partial x} \tag{4.1b}$$

$$\frac{\partial u}{\partial t} = c \frac{\partial w}{\partial x} - c(\gamma-1) \frac{\partial e}{\partial x} \tag{4.1c}$$

(4.1a) is the energy equation, (4.1b) is the continuity equation, and (4.1c) is the momentum equation. Here the dependent variable u is the velocity and is assumed to be small since sound waves are being considered. e is ε/c where ε represents a small perturbation of the internal energy from an ambient state ε_o, and c is a constant scaling factor equal to the isothermal sound speed of the ambient state. w is cV/V_o where V is a small perturbation of the specific volume from the ambient value V_o. In (4.1), γ is the usual gas constant and $\sigma \equiv k/\rho_o c_v$, where k is the thermal conductivity, ρ_o is the ambient density, and c_v is the specific heat at constant volume.

For the numerical tests, the interval of interest was $0 \leq x \leq 1$, and the boundary conditions were

$$u(0) = u(1) = \left.\frac{\partial e}{\partial x}\right|_{x=0} = \left.\frac{\partial e}{\partial x}\right|_{x=1} = 0.$$

For a perfect gas e is directly proportional to the temperature, which means that the conditions on e are equivalent to no heat conduction out of the region of interest. The spatial discretization used was based on the uniform staggered grid illustrated in Figure 4.1

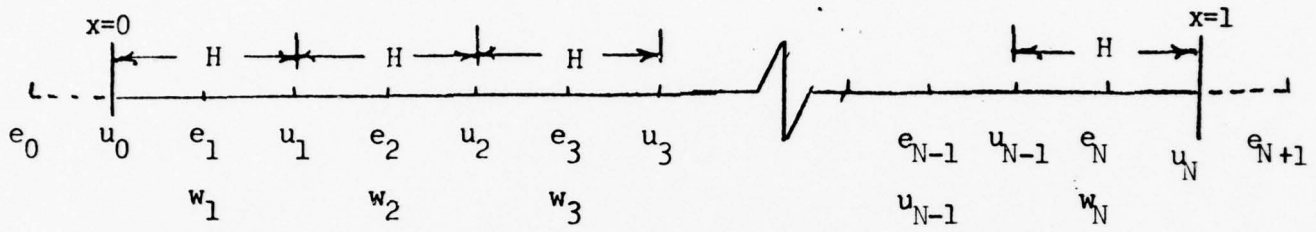

Figure 4.1. Staggered Grid

For convenience, we have introduced fictitious quantities e_o and e_{N+1}, which will be eliminated shortly by means of boundary conditions. Now discretizing in the obvious way we obtain the ordinary differential system:

$$\begin{pmatrix} \dot{e}_1 \\ \dot{w}_1 \\ \dot{u}_1 \\ \dot{e}_2 \\ \dot{w}_2 \\ \dot{u}_2 \\ \vdots \\ \dot{e}_{N-1} \\ \dot{w}_{N-1} \\ \dot{u}_{N-1} \\ \dot{e}_N \\ \dot{w}_N \end{pmatrix} = \begin{pmatrix} \sigma(e_2 - 2e_1 + e_o)/H^2 - c(u_1 - u_0)/H \\ c(u_1 - u_0)/H \\ c(w_2 - w_1)/H - c(\gamma-1)(e_2 - e_1)/H \\ \sigma(e_3 - 2e_2 + e_1)/H^2 - c(u_2 - u_1)/H \\ c(u_2 - u_1)/H \\ c(w_3 - w_2)/H - c(\gamma-1)(e_3 - e_2)/H \\ \vdots \\ \sigma(e_N - 2e_{N-1} + e_{N-2})/H^2 - c(u_{N-1} - u_{N-2})/H \\ c(u_{N-1} - u_{N-2})/H \\ c(w_N - w_{N-1})/H - c(\gamma-1)(e_N - e_{N-1})/H \\ \sigma(e_{N+1} - 2e_N + e_{N-1})/H^2 - c(u_N - u_{N-1})/H \\ c(u_N - u_{N-1})/H \end{pmatrix} \tag{4.2}$$

Note that $\dot{u}_0$ and $\dot{u}_N$ do not appear in the derivative vector since they are required to be zero by the boundary conditions. By the same token it is understood that u_0 and u_N are replaced by zero on the RHS of (4.2). The boundary conditions on e are approximated by $e_0 = e_1$ and $e_{N+1} = e_N$. Using these to eliminate e_0 and e_{N+1} from the RHS of (4.2), we have a system of (3N-1) ordinary differential equations. Of course, to complete the problem, we must specify initial conditions for the (3N-1) dependent variables.

In performing the spatial discretization to obtain this ordinary differential system, all of the partial differential equations and boundary conditions were replaced by finite difference approximations of second order accuracy. Consequently, the difference between the solution to (4.2) and the solution to (4.1) (evaluated at the mesh points) can be expected to be $O(H^2)$. Now if a nonuniform mesh were desired, it would not be possible to generalize (4.2) to such a mesh and still maintain 2nd order accuracy. Alternatively, one might try a conventional nonuniform mesh for which all the nodal variables with the same subscript (u_i, w_i, e_i) all correspond to the same spatial point. By replacing all first and second derivatives with respect to x by appropriate difference quotients, a second order approximation would be obtained. However, in such a scheme, approximations to first derivatives would involve three consecutive nodal values. This is not objectionable if there is also second derivative term present in the same equation. However, if there are no second derivatives present, as in (4.1b) and (4.1c), this procedure is perilous and will probably result in an ordinary differential system with spurious growing solutions. This phenomenon was discussed in the preceding section in connection with appropriate spatial discretization of the Blasius boundary layer equations. Fortunately, there is another finite difference scheme which could be used on (4.1) and which is quite convenient for nonuniform meshes. It is sometimes referred to as the "box" method (Keller [12]). This differencing method is illustrated in Section IV.C.1. It has not been used on (4.1) but there would be no difficulty in doing so.

For the test cases, the constants σ, c, and γ were set to 1., 1., and 1.4, respectively. With these values for the constants, an exact solution to (4.1) is:

$$\begin{Bmatrix} e(t) \\ w(t) \\ u(t) \end{Bmatrix} = A_1 \begin{Bmatrix} \cos 2\pi x \\ .01008\cos 2\pi x \\ -.06268\sin 2\pi x \end{Bmatrix} e^{-39.08t}$$

$$+ \begin{Bmatrix} \cos 2\pi x \\ -.8050\cos 2\pi x \\ -6.252\sin 2\pi x \end{Bmatrix} (A_2 \cos 6.312t + A_3 \sin 6.312t) e^{-.1969t}$$

$$+ \begin{Bmatrix} 0. \\ 6.249\cos 2\pi x \\ -1.005\sin 2\pi x \end{Bmatrix} (-A_2 \sin 6.312t + A_3 \cos 6.312t) e^{-.1969t} \qquad (4.3)$$

In (4.3) A_1, A_2, and A_3 are arbitrary constants. Another exact solution can be obtained by reversing the roles of $\sin 2\pi x$ and $\cos 2\pi x$ and reversing the sign of the last element in each of the braces on the RHS. However, the one displayed in (4-3) is the one of interest since it satisfies the boundary conditions, $u(0) = u(1) = \left.\frac{\partial e}{\partial x}\right|_{x=0} = \left.\frac{\partial e}{\partial x}\right|_{x=1} = 0$, which, as noted earlier, are the ones to be incorporated into the finite difference spatial discretization. For the test problem, we chose $A_1 = 1.$, $A_2 = A_3 = 0$. With this choice of the A_i, (4.3) was then evaluated (with $t = 0$) at the mesh points of the finite difference grid to get the initial conditions for the ordinary differential system (4.2). GEARIB was then used to integrate (4.2) with the accuracy parameter, ε, set to 10^{-6}, which is adequately small considering the accuracy of the spatial discretization. Two different spatial mesh sizes were used, $H = 1/30$ and $H = 1/60$. Now with $A_2 = A_3 = 0$ in (4.3), the exact solution is a rapidly decaying exponential in time. Thus, after a short time the solution of (4.2) should be very small. The extent to which it is not is a measure of the error. Comparing this error for the two different mesh sizes, it was found that the error for $H = 1/60$ was about 1/4 of that for $H = 1/30$, exactly what theory would predict. Further, the errors themselves behaved very much like the two terms containing A_2 and A_3 on the right of (4.3). The reason for this is that the initial condition for (4.2) which would excite only a rapidly decaying exponential solution (the finite difference counterpart of the first term on the right of (4.3)), is not exactly $\cos 2\pi x$ evaluated at the mesh points. Because this "non-exact" initial condition was used, small amounts of the finite difference counterparts of the 2nd and 3rd terms on the right of (4.3) were excited, and these components die out rather slowly. (Possibly the initial condition excited small components corresponding to higher spatial harmonics, e.g., $\cos 4\pi x$, but these were not present in noticeable amounts.)

Because of the smoothness of the solution, GEARIB integrated most of the way with a 4th and 5th order method, with the stepsize gradually increasing as the slowly decaying component became smaller.

We note that Richtmyer and Morton [11] have developed a combined implicit-explicit method for the numerical solution of (4.1) ((4.1a) is treated implicitly because of the diffusion term). Although much better than a purely explicit method, there is still a stability limitation, i.e., Δt must be less than a certain involved function of Δx, c, and σ. At the end ($t = 2.5$) of the numerical example discussed above, the Δt being used by GEARIB exceeded the maximum allowed by Richtmyer and Morton's method by a factor of about 4.5. If the integration had proceeded further or if a larger value of ε had been used, GEARIB would compare even more favorably. On the other hand, for solutions that decay less rapidly the advantage of GEARIB would be less clear. For example, the initial condition

$$e(x) = \cos 2\pi x, \quad u(x) = w(x) = 0 \tag{4.4}$$

which does not appear to be much different than that of the preceding discussion, excited very significant components of the finite difference counterparts of the

2nd and 3rd terms of (4.3). Consequently, the solution decayed slowly. At t = 2.5, for example, the integration step size, Δt, was less than 1/10 of that of the example discussed earlier, and Δt was well within the Richtmyer-Morton limit.

C. Burger's Equation

For the initial tests of GEARIB used in conjunction with the "Box" scheme for spatially discretizing PDE's, Burgers equation,

$$\frac{\partial T}{\partial t} = \beta \frac{\partial^2 T}{\partial x^2} - \gamma T \frac{\partial T}{\partial x} \tag{4.5}$$

was chosen. This is a favorite PDE to test numerical schemes with since by varying the relative magnitudes of the constants β and γ either the diffusive effect or the nonlinear wave effect can be emphasized. (Setting γ to zero yields the one-dimensional diffusion equation.) Swartz and Wendroff [13] and Sincovec and Madsen [14] have tested their numerical methods on (4.5). The latter reference also contains an exact solution, which was taken from Cole [15]. Cole also discusses different physical interpretations of the dependent variable T of (4.5). Perhaps, the most relevant interpretation for the present study is that of a simplified model of a traveling structured shock where T is to be regarded as a "generalized velocity."

C.1 Application of the "Box" Differencing Scheme to Burger's Equation

In this section, we discuss the application of the box differencing scheme to Burger's equation. (The term "box" was used by Isaacson [16] and later Keller [12]. Their use of this term is more specific than we are using it. They require that the marching scheme in time be the trapezoidal rule, whereas we allow it to be chosen automatically by GEARIB from a class of backward difference formulas.) We also give a detailed discussion of certain precautions required in the selection of initial conditions. Most of these ideas extend to the more complicated PDE's to be discussed later in this report.

To use the Box scheme, it is necessary to express (4.5) as a system of first order (in x) ODE's. First introduce

$$v \equiv \frac{\partial T}{\partial x} \tag{4.6}$$

Then (4.5) can be replaced by,

$$\frac{\partial T}{\partial t} = \beta \frac{\partial v}{\partial x} - \gamma v T \tag{4.7a}$$

$$0 = v - \frac{\partial T}{\partial x} \tag{4.7b}$$

The boundary conditions are assumed to be separated but otherwise quite general, i.e.,

$$g_1(T_1, v_1, t) = 0, \quad g_N(T_N, v_N, t) = 0, \tag{4.8}$$

where g_1 and g_N are arbitrary functions continuous in t, and the subscripts 1 and N refer to the left and right boundaries.

Now assume a finite difference mesh with nodes at $x_1, x_2, \ldots, x_N$, with T_i and v_i associated with x_i, and $H_i \equiv (x_{i+1} - x_i)$. Then replacing (4.7) by finite differences in the obvious way we get the following differential algebraic system:

$$\begin{bmatrix} 0 & 0 & 0 & 0 & 0 & \cdots & \cdots \\ .5 & 0 & .5 & 0 & 0 & & \\ 0 & 0 & 0 & 0 & 0 & & \\ 0 & 0 & .5 & 0 & .5 & & \\ 0 & 0 & 0 & 0 & 0 & & \\ \vdots & & & & & & \\ & & & & & .5 & 0 & .5 & 0 \\ & & & & & 0 & 0 & 0 & 0 \\ & & & & & 0 & 0 & 0 & 0 \end{bmatrix} \begin{Bmatrix} \dot{T}_1 \\ \dot{v}_1 \\ \dot{T}_2 \\ \dot{v}_2 \\ \dot{T}_3 \\ \vdots \\ \dot{T}_{N-1} \\ \dot{v}_{N-1} \\ \dot{T}_N \\ \dot{v}_N \end{Bmatrix} = \begin{Bmatrix} g_1(T_1, v_1, t) \\ \beta(v_2 - v_1)/H_1 - \gamma(v_1 T_1 + v_2 T_2)/2 \\ (v_1 + v_2)/2 - (T_2 - T_1)/H_1 \\ \beta(v_3 - v_2)/H_2 - \gamma(v_2 T_2 + v_3 T_3)/2 \\ (v_2 + v_3)/2 - (T_3 - T_2)/H_2 \\ \vdots \\ \beta(v_N - v_{N-1})/H_{N-1} - \gamma(v_{N-1} T_{N-1} + v_N T_N)/2 \\ (v_{N-1} + v_N)/2 - (T_N - T_{N-1})/H_{N-1} \\ g_N(T_N, v_N, t) \end{Bmatrix} \tag{4.9}$$

Note that the matrix multiplying the derivative vector is singular, so it is in general not possible to solve for these derivatives. (In fact, the coefficients of the $\dot{v}_i$ are all zero.) Consequently, (4.9) could not be solved as it stands using conventional integration routines.

For typical problems, g_1 would be a simple function, e.g., $T_1 - f(t)$, where f(t) is a prescribed function of time, often constant. (Similarly, for g_N.) In such cases, T_1 (T_N) could be eliminated from (4.9) entirely, thus reducing the

order of the system by 2. For generality, we choose not to do this. In later sections, examples are given using complicated nonlinear functions for g_1 and g_N.

To complete the specification of the problem governed by (4.9) initial conditions must be supplied. From the physical problem values of T_i at t=0 would be known, but the initial v_i may not be given. Now it may well be that the v_i are never actually of interest, but are to be regarded only as convenient auxiliary variables. In this case, the question of how to set the initial v_i arises. In principle, they could be set arbitrarily. This can be seen as follows: In GEARIB the starting method is the backward Euler method, i.e., (4.9) is written at $(t_o + h)$ replacing $\dot{T}_i$ by $(T_i(t_o + h) - T_i(t_o))/h$, and similarly with $\dot{v}_i$. (Here t_o is the initial time and h is the time step.) (4.9) has become a system of 2N nonlinear equations for the 2N unknowns, $T_1(t_o + h)$, $v_1(t_o + h)$, ..., $T_N(t_o + h)$, $v_N(t_o + h)$. The solution of this system depends on the initial values of the T_i by virtue of the backward difference formula used to approximate $\dot{T}_i$. However, as noted earlier, the $\dot{v}_i$ do not actually appear in (4.9). Consequently, the solution of the nonlinear system does not depend on the initial v_i.

In practice, however, since this nonlinear system is going to be solved by a quasi-Newton method, it is desirable to start this iterative process from a "point" (in the 2N-space $(T_1,v_1,\ldots,T_N,v_N)$) which is not too much different from the solution. Now since the T_i change continuously in time from their initial values and since the initial step size h is small, it is reasonable to use the initial T_i for N of the starting point coordinates. (Actually, even better values of T_i are obtained by using an explicit prediction from the initial T_i, but this requires a knowledge of the initial $\dot{T}_i$, which may not be available. More on this later.) To select the initial v_i, observe that after the first step, the 3rd, 5th, ..., (N-1)th equations, which are strictly algebraic, will be satisfied exactly (to within the convergence criterion of the quasi-Newton method). Since the T_i don't change very much over the first short step, a reasonable requirement is that the initial v_i satisfy these algebraic equations initially. Since these equations are linear, it may be a simple matter to do this, i.e.,

$$\begin{aligned} v_2 &= 2(T_2 - T_1)/H_1 - v_1 \\ v_3 &= 2(T_3 - T_2)/H_2 - v_2 \\ &\text{etc.} \end{aligned} \tag{4.10}$$

If v_1 or v_N are prescribed, (4.10) provides a unique solution for the v_i. If both v_1 and v_N are assigned, (4.10) is overdetermined and there is no solution unless the T_i satisfy a certain compatibility condition. This restriction is easily obtained by adding the algebraic equations of (4.9) (after multiplying each equation by its respective H_i):

$$T_1 - T_N = \sum_{i=2}^{N} H_{i-1}(v_{i-1} + v_i)/2 \tag{4.11}$$

At first it might seem contradictory to require such a condition on the T_1, which ought to be prescribable arbitrarily. However, it is unreasonable to choose an initial profile for T which is not consistent (or nearly so) with the prescribed values of v_1 and v_N (which approximate $\partial T/\partial x$ at x_1 and x_N). Such an inconsistent T profile is tantamount to changing the boundary conditions discontinuously at t_o^+ (from boundary conditions consistent with the initial T profile to those actually prescribed). For such problems, T_1 and T_N would undergo large changes during the first step, so that (4.11) would be satisfied after the first step. In this situation, it is not clear how the initial v_i should be set, but it may not matter much since T_1 and T_N (and probably other T_i) change so violently. We exclude such pathological problems from further consideration.

If both T_1 and T_N are prescribed boundary conditions then there is one degree of freedom in the solution for the initial v_i from (4.10). To set this degree of freedom we refer back to system (4.9). Since T_1 and T_N are prescribed, $\dot{T}_1$ and $\dot{T}_N$ are known (possibly functions of time). With $\dot{T}_1$ known, $\dot{T}_2$ can be obtained directly from the 2nd equation of (4.9) in terms of elements of the RHS (which depend on the one degree of freedom in the solution for the initial v_i). Likewise, $\dot{T}_3$ can be obtained from the 4th equation in terms of $\dot{T}_2$ and the RHS. This process can be continued to the (N-3)rd equation, which yields an expression for $\dot{T}_N$. But $\dot{T}_N$ is already known. Thus, the remaining degree of freedom in the solution for the v_i is chosen to make these two expressions for $\dot{T}_N$ consistent. What if this degree of freedom is chosen differently? For the moment, assume that the initial integration step, h, is small enough so that the $T_i(t_o + h)$ and $v_i(t_o + h)$ are not too much different than their initial values. Replacing the time derivatives by backward differences we can approximately solve for $T_2(t_o + h)$ from the 2nd equation, $T_3(t_o + h)$ from the 4th, etc. Finally, the (N-3)rd equation gives an expression for $T_N(t_o + h)$, which is already known from the boundary condition. If the initial conditions for the v_i were chosen as discussed above, then these two expressions for $T_N(t_o + h)$ will be nearly consistent. These two equations (and in fact the whole system of 2N equations) can be made consistent by a slight readjustment of the v_i (which is done automatically by the Newton iterations). However, if the initial v_i were not chosen as described above, then the $v_i(t_o + h)$ will undergo a violent readjustment in order that a solution to the system of 2N equations be possible.

In the preceding paragraphs, we have discussed the choice of initial conditions when the boundary condition function g_1 of (4.9) involved only T_1 or v_1 (and similarly with g_N). The criterion used was that the initial conditions should be chosen so that none of the T_i or v_i change drastically during the first step, since this could jeopardize the convergence of Newton's method for $T_i(t_o + h)$ and $v_i(t_o + h)$. For more complicated boundary condition functions, g_1 and g_N, such a compatibility analysis is likely to become more involved. Further, more complicated systems of partial differential equations, which are examined later in this report, compound such analyses. It would be nice if a foolproof automatic method of starting the integration were available. However, this is probably asking too much. For example, consider the extreme case where the system to be solved was purely algebraic, i.e., the derivative matrix analogous to that of (4.9) contained only zeroes. In order that the solution variables change in time (like those of a differential system) there would have to be at least one time dependent function or coefficient embedded in the algebraic system. (Such problems are readily treated using GEARIB.) If

initial conditions satisfying the algebraic equations at t_o were unknown, they would have to be obtained by an iterative scheme, e.g., Newton's method (assuming that the algebraic system is nonlinear). Since there is no known foolproof method for solving a nonlinear system starting from an arbitrary initial guess, it is not possible to make the starting process automatic for arbitrary differential-algebraic systems. About the best that can be done is to choose the initial conditions as reasonably as possible (in lieu of a complete analysis of a type described earlier in this section) and to use a good iterative method. In the case of (4.9) this might be:

i) Choose the v_i to satisfy (4.10).

ii) If there is still a degree of freedom left in this solution, fix it in some reasonable manner, e.g., by computing a 3-point forward difference approximation to $\partial T/\partial x\Big|_{x=x_1}$ and setting v_1 to this value, which is the additional condition needed to make the initial v_i unique.

iii) Use a strict Newton method (instead of the less reliable, but more efficient quasi-Newton method employed in GEARIB) for the first step.

Once the GEARIB integration is underway, the first phase of advancing the solution from the current time t_n to $(t_n + h)$ is to use an explicit prediction (based on the derivatives at t_n) to approximate the dependent variables at $(t_n + h)$, which is then used as a starting point for the quasi-Newton iteration for the solution at $(t_n + h)$. This approach almost always reduces the number of quasi-Newton iterations for convergence. The same thing could be done for the first step, providing the initial derivatives can be computed. If the derivative matrix on the left of (4.9) were non-singular, then GEARIB contains an option for solving for these initial derivatives. Unfortunately, as noted earlier, this matrix is clearly singular. However, if the algebraic equations are differentiated and moved to the LHS of (4.9), the matrix may or may not be singular. If T_1 and v_N (or v_1 and T_N) are prescribed, then the modified matrix is non-singular and the initial derivatives can be obtained by GEARIB. However, if T_1 and T_N or v_1 and v_N are prescribed, this matrix is singular. There is a solution for the initial derivatives only if the initial T_i and v_i are compatible, as discussed earlier in this section. If they are compatible, it is necessary that the user supply a special subroutine which computes these initial derivatives. In most of the cases run, it was unnecessary to do this. The initial derivatives were arbitrarily set (usually to zero) in the user supplied subroutine, and if the initial step was relatively small, the quasi-Newton method would usually converge inspite of the bad prediction (based on the arbitrarily chosen initial derivatives). Unfortunately, in those cases where it is difficult to solve for the initial derivatives (because of a singular derivative matrix - even after differentiation of the algebraic equations), the Newton matrix becomes singular as $h \to 0$. For these cases, there must be some compromise on the initial h. It must be small enough so that a bad prediction (based on incorrect initial derivatives) will not jeopardize convergence of the Newton (or quasi-Newton) iteration. On the other hand, if the initial h is too small, the factorization of the Newton matrix will be inaccurate and the Newton iteration may fail to converge for that reason. Generally, the selection of a

suitable initial h was not a problem, but it could have been if the computations had been performed in single precision.

In the preceding paragraph, we cited an advantage of basing the integration on a purely differential system (obtained by differentiating all algebraic equations) instead of using the original differential-algebraic system (4.9). A disadvantage might seem to be the extra work required of the user to put the system in the modified form (by analytically differentiating the algebraic equations). This may or may not be true depending on the following considerations: To use Newton's method in conjunction with GEARIB, it is necessary to form the Jacobian matrix corresponding to the right hand side vector of (4.9). GEARIB provides two options for doing this. In the first option the user obtains analytical formulas for the elements of Jacobian and codes these formulas into a user supplied subroutine. In the second option, GEARIB computes these elements using numerical differencing techniques. The second option is more convenient for the user, but usually requires somewhat more CPU time, and sometimes the error introduced by the numerical differencing affects the integration adversely in that convergence of the Newton iteration is slower, which results in a further increase of CPU time. This is especially true if high accuracy is demanded of the integration. If the analytical Jacobian option is to be used, then differentiating the algebraic equations does not increase the analytical work on the part of the user, since the algebraic equations disappear from the RHS thus reducing the complexity of the formulas for the Jacobian of the RHS, but this reduction in work is compensated for by the increased complexity of the matrix multiplying the derivative vector on the left. If the numerical Jacobian option is used, then differentiating the algebraic equations does result in extra analytical work by the user.

There is another advantage in using the differential-algebraic form. By differentiating algebraic equations, information is lost in a sense. This effect was actually seen in numerical experiments in which the same problem was solved using both the differential-algebraic and the purely differential systems. The former almost always gave somewhat more accurate answers.

C.2 Results of Numerical Tests with Burger's Equation

For simplicity, the first numerical tests of the Box method were carried out on the diffusion equation (obtained from (4.5) by setting γ to zero). For these tests (and all tests with the full Burger's equation), the x interval was [0,1] which was subdivided into 40 equally spaced intervals. Recall that the discretized Burger's equation (4.9) was written for nonuniform meshes, and such meshes could have been used in our tests with very little extra effort, had it been warranted.

In the first test with the diffusion equation, the boundary conditions were $\partial T/\partial x = 0$ at both ends, or, equivalently, $v_1 = v_N = 0$. The initial condition for the T_i was taken from $\cos\pi x$ evaluated at the mesh points. The initial v_i were then computed from (4.10) starting with $v_1 = 0$. v_N was not computed using (4.10), which probably would have yielded a small non-zero value for v_N. Instead, the initial v_N was set to 0, its prescribed boundary value. This slight inconsistency did not cause any starting problems and the integration proceeded as expected, using 3rd and 4th order methods most of the way and giving good agreement with the exact solution, which is:

$$T(x,t) = e^{-\beta\pi^2 t}\cos\pi x, \tag{4.12}$$

and v(x,t) being the x-derivative of T(x,t). ($\beta = 1$ for all tests with the diffusion equation.)

For the second set of tests with the diffusion equation, the boundary conditions were $T_1 = 1$, $T_N = 0$. The initial condition for the T_i was taken from

$$T(x) = \begin{cases} 1, & x \leq c \\ .5[1 + \cos(\pi(x-c)/L)], & c < x < (1-c) \\ 0, & x \geq (1-c) \end{cases} \tag{4.13}$$

The constant c must satisfy $0 \leq c < 1/2$ and $L \equiv 1-2c$. An exact solution to the continuous problem can be obtained by Fourier series methods:

$$T(x,t) = (1-x) + \sum_{n=1}^{\infty} a_n \sin(2\pi nx)e^{-4\pi^2 n^2 t}, \tag{4.14a}$$

where

$$a_n = \frac{\cos(2\pi nc)}{\pi n(4n^2L^2-1)} \tag{4.14b}$$

If $L = 1/2n$ for some n, (4.14b) is an indeterminate form and must be evaluated differently. In our examples we avoid this case. For the first example, c=0. Now since $\gamma=0$, (4.9) is linear, which in turn means that the algebraic system resulting from (4.9) (after replacing the time derivatives by backward difference approximations) is also linear. Thus, Newton's method will converge in only one iteration on the first step regardless of the initial choice of v_i and the initial values of $\dot{v}_i$ and $\dot{T}_i$ used for the prediction. (This is not necessarily true on subsequent steps since the integration step size, h, upon which the Newton matrix depends, can be changed by GEARIB without a corresponding change in the Newton matrix and its factors, i.e., the quasi-Newton method.)

The principal difficulty with this problem is that v undergoes very rapid changes for small values of t near x=c and x=1-c. This can be seen by differentiating (4.14a) with respect to x and t, i.e.,

$$\dot{v} \equiv \frac{\partial^2 T}{\partial x \partial t} = \sum_{n=1}^{\infty} - a_n(2\pi n)^3\cos(2\pi nx)e^{-4\pi^2 n^2 t} \tag{4.15}$$

Now substitute t=0, x=c, and (4.14b) for a_n:

$$\dot{v}(c,0) = \sum_{n=1}^{\infty} \frac{-\cos^2(2\pi nc)(2\pi n)^3}{\pi n(4n^2L^2-1)}, \qquad (4.16)$$

which does not converge, i.e., $\dot{v}(c,0)$ is singular in the continuous problem, and we can expect very rapid changes in the corresponding value of v_i in the discretized problem. Now rapid changes in the v_i are not in and of themselves harmful since $\dot{v}_i$ does not appear in the differential-algebraic system (4.9). However, because of the design of GEARIB (which has no provision for detecting the absence of the derivative of a particular dependent variable) such rapid changes in the v_i can exert a strong influence on the progress of the integration. This can be seen as follows:

Once the Newton iteration converges (in the course of advancing the solution to the next time point), GEARIB estimates the error committed for each dependent variable during the step. This error is due to the replacement of the time derivatives in the original system by backward difference formulas. For example, the method used for the first two steps (and possibly more) is the backward Euler. According to theory, the error committed during one step in T_i, say, using the backward Euler is $O(h^2\ddot{T}_i)$. $\ddot{T}_i$ is estimated by GEARIB as $[\dot{T}_i(t_o + h) - \dot{T}_i(t_o)]/h$, where $\dot{T}_i(t_o + h) = [T_i(t_o + h) - T_i(t_o)]/h$, i.e., just the backward difference approximation of the backward Euler method. ($\dot{T}_i(t_o)$ is just the value of the initial derivative supplied by the user or computed automatically by GEARIB if the derivative matrix is non-singular.) Since GEARIB is "unaware" of the missing $\dot{v}_i$, the same error estimates will be computed for each of the v_i. A large change in v_i (from $v_i(t_o)$ to $v_i(t_o + h)$) for one or more values of i may result in an error estimate by GEARIB which violates the user supplied accuracy requirement. Consequently, the step size, h, will be reduced and the step retried until the accuracy criterion is satisfied. To avert this spurious reduction in h resulting from rapid changes in some of the v_i, GEARIB was modified so that v_i would not be included in the error test.

From the preceding discussion, it is seen that even when the v_i error test is suppressed there may still be trouble with the error test on the first step if incorrect values of $\dot{T}_i(t_o)$ are supplied. (Because of the linearity of the problem currently under discussion, the prediction has no bearing on the convergence of Newton's method and these initial derivatives are irrelevant from this standpoint.) Unless the values of $\dot{T}_i(t_o)$ are correct (see discussion in the following paragraph) then GEARIB should be modified so that the error test on the T_i is suppressed for the first step. In this situation, it is up to the user to choose a conservatively small initial h so as not to incur an excessive error on the first step.

In our numerical experiments, two different starting techniques were used. For the first arbitrary initial values for $\dot{v}_i$ and $\dot{T}_i$ were supplied and the error test was completely suppressed for the first step. For the second, the initial $\dot{T}_i$ were computed based on a "compatible" selection of the initial v_i (as discussed

in the preceding subsection). The initial step was taken suppressing the error test on the v_i. The first approach is certainly the simpler, but the second is more reliable. After the first step, the error test was in effect for T_i but not v_i (regardless of the starting method). As it turned out, in these particular examples the results were quite similar. As noted earlier $\dot{v}_1(c,t)$ is singular in the continuous solution. This singularity is also felt by the T_i (but less strongly), and despite the suppression of the error test on v_i, the relatively large values of T_i restricted the build up of step size during the early stages of the integration. Beyond this the integration behaved as expected.

Another case was run with $c = .4$. The results were not essentially different although the integration took somewhat longer due to the steeper initial spatial derivatives (due to this choice of c). In all cases, the numerical solution agreed satisfactorily with the exact solution (computed from the Fourier series).

Several different examples were tried with the full Burger's equation, (4.5) with $\beta = \gamma \neq 0$. For all these tests $\gamma = 1.$, and β was varied from 10^{-4} to 1. The boundary conditions were $T_1 = 1$, $T_N = 0$. Expression (4.13) with $c = .4$ or .475 was used for the initial T_i, and the initial v_i were computed from (4.10) using a compatible value for v_1 (as discussed in the preceding section). Although the "correct" initial values for T_i could have been computed (since the initial v_i were compatible) this was not done. Note that in the nonlinear problem it could be important to have good initial derivatives since the Newton process will not necessarily converge in one iteration as in the purely diffusive case. However, it is probably even more important to have the initial v_i consistent with the initial T_i (which was done) which should help the Newton process converge.

In the numerical tests, it turned out that the $\beta = \gamma = 1$ case was nearly the same as the purely diffusive problem $\beta = 1.$, $\gamma = 0$. Although the v_i changed very rapidly for small t, there was no problem with the convergence of the Newton process. For smaller values of β (maintaining $\gamma = 1.$), the diffusive effect was weak and v_i did not undergo rapid initial changes. Plotted in Figure 4-2 are T-profiles for various values of t for the $\beta = 10^{-4}$, $\gamma = 1.$ case.

There are several things to be noted from Figure 4-2. Because the diffusive effects are so weak, the initial profile begins steepening almost immediately and after a short time assumes its "asymptotic" shape and from then on travels practically undistorted at a constant velocity. (Because of the finiteness of the right hand boundary this cannot, of course, go on indefinitely.) Another feature to notice is the appearance of spurious oscillations in the trough of the wave. Similar phenomena have been encountered by other workers. For example, in the calculations of Schwartz and Wendroff [13], using a different spatial discretization, spurious oscillations appeared at the crest of the wave. They point out that from theoretical considerations the asymptotic wavelength is $O(10\beta)$ and if the spatial mesh (here .025) is greater than this wavelength one should not be surprised at such oscillations. When computations were made with larger values of β, these oscillations became smaller and disappeared altogether. One run was made with a steeper initial profile ($c = .475$ in the definition of the initial T_i in (4.13)). Because of the increased steepness of the initial profile, the integration proceeded somewhat more slowly than for the initial profile illustrated in Figure 4-2. Also,

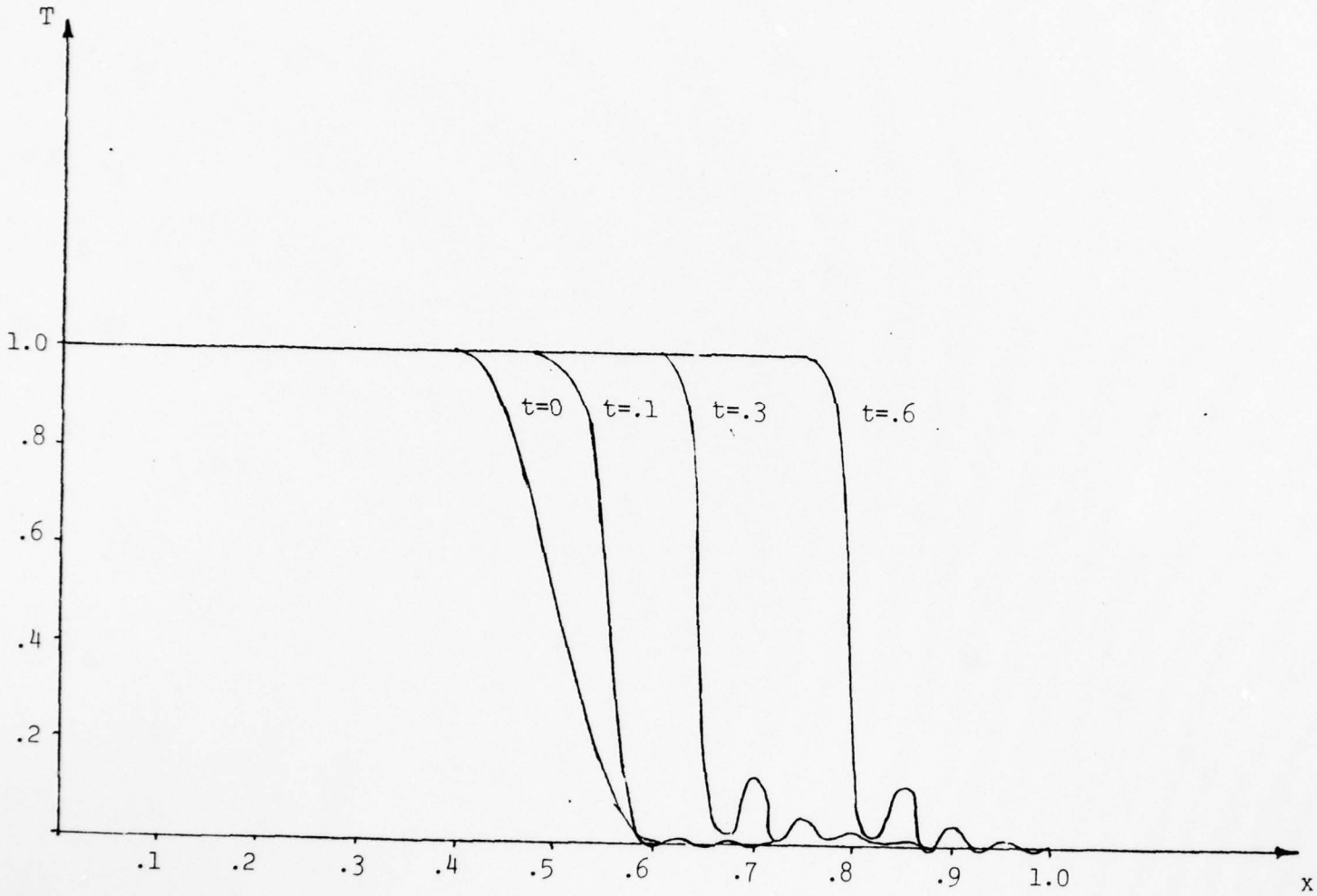

Figure 4.2 T-Profiles for Burgers Equation ($\beta = 10^{-4}$, $\gamma = 1.$)

the spurious oscillations appeared sooner. However, the asymptotic behavior of the solution seems to depend very little on the initial profile.

Although there are some exact solutions available for special initial conditions (see Sincovec and Madsen [14] or Cole [15]), there does not appear to be any corresponding to the initial conditions (4.13) used in this study. Qualitatively, our results are in agreement with those of Schwartz and Wendroff [13] and Sincovec and Madsen [14].

V. ONE-DIMENSIONAL UNSTEADY GAS FLOW

A. Introduction

In this section the application of the GEARIB integration method in conjunction with the box method of spatial discretization to a variety of one-dimensional unsteady gas flow problems is discussed. Many of the numerical difficulties encountered in the solution of these problems are also expected to be present in realistic unsteady laser flows. Thus, the present work is a necessary first step in the development of a comprehensive unsteady laser simulation program.

B. Governing Equations

In this subsection we list the governing partial differential equations for one-dimensional unsteady gas flow. These equations contain provisions for a variety of different gas flow phenomena, e.g., heat and mass injection, wall friction, dissipation, etc. All problems subsequently examined in this section are governed by appropriate specializations of these partial differential equations. These PDE's are also consistent (but with somewhat different notation) with the PDE's governing the quasi one-dimensional steady laser flows used in the BLAZE-II program (Sentman, Subbiah, and Zelazny [17]). The equations listed here are more general in the sense that they contain time dependent terms plus certain others, e.g., dissipation, heat conduction, etc., but are less general in that they do not provide for chemical reactions and radiation, which are essential to laser simulations. The governing equations are listed below in the order; continuity, momentum, energy, and gas law; with all unknown time derivatives appearing on the left.

$$
\begin{bmatrix} 1 & 0 & 0 & 0 \\ 0 & 1 & 0 & 0 \\ 0 & 0 & (-1/\rho c_p) & 1 \\ 0 & 0 & 0 & 0 \end{bmatrix}
\begin{Bmatrix} \dot{\rho} \\ \dot{u} \\ \dot{p} \\ \dot{T} \end{Bmatrix}
=
\begin{Bmatrix}
[M - \rho u \frac{\partial A}{\partial x} - \rho \dot{A}]/A - \rho \frac{\partial u}{\partial x} - u \frac{\partial \rho}{\partial x} \\
- u \frac{\partial u}{\partial x} - \frac{1}{\rho} \frac{\partial p}{\partial x} - \frac{(u-u_M)M}{\rho A} + F + \frac{F_N}{\rho A} + \frac{\mu}{\rho} \left[\frac{4}{3} \frac{\partial^2 u}{\partial x^2} + \frac{1}{A} \frac{\partial u}{\partial y} \Big|_{y_L}^{y_U} \right] \\
- u \frac{\partial T}{\partial x} + \frac{u}{\rho c_p} \frac{\partial p}{\partial x} + \frac{(H_M - H)M}{\rho c_p A} + \frac{Q}{\rho c_p A} + \frac{k}{\rho c_p} \frac{\partial^2 T}{\partial x^2} \\
\quad + \frac{u}{\rho c_p A} [(u_M - u)M + F_N] + \frac{\mu}{\rho c_p} \left[\frac{4}{3} \left(\frac{\partial u}{\partial x} \right)^2 + \frac{1}{A} \int_{y_L}^{y_U} \left(\frac{\partial u}{\partial y} \right)^2 dy \right] \\
p - \rho R T
\end{Bmatrix}
\tag{5.1}
$$

The notation employed in (5.1) is defined:

x axial coordinate

y transverse coordinate (varies from y_L to y_U)

ρ density

u axial velocity

p pressure

T temperature

A duct cross-sectional area which is assumed to be a prescribed function of x and t. (A could even depend on ρ, u, p, and/or T but then the form of (5.1) would change according to the particular form of this relation. We do not consider this here although there would be no difficulty in doing so.)

M rate (per unit axial length per unit time) of mass injection through the duct wall

u_M x-component of velocity of injected mass

v_M y-component of velocity of injected mass

F body force (conservative)

F_N friction force (per unit axial length) at a non-slip wall. If F_N is included the last term of the momentum equation (involving $\mu\, \partial u/\partial y$) should be omitted. This latter term is used for problems with partial slip boundaries for which the friction force performs work. We do not consider partial slip boundaries in this report, but they are important in the quasi-one-dimensional analysis of the BLAZE-II program [17].

μ coefficient of viscosity. Note the factor (4/3) multiplying μ when applied to the x-derivatives of u. For a careful discussion of this point see von Mises [18], p. 136.

c_p specific heat at constant pressure

H total enthalpy of fluid ($\equiv c_p T + u^2/2$)

H_M total enthalpy of injected mass ($\equiv c_p T_M + u_M^2/2 + v_M^2/2$)

Q rate (per unit axial length per unit time) of heat addition through the duct wall

k coefficient of thermal conductivity

R gas constant

For the numerical results presented later in this section, the following values were used:

c_p = 1000. (joule/kilogram degree)

R = 286.7 (joule/kilogram degree)

μ = various values (newton second/meter^2)

k = 0

Also, using the formula, $\gamma = c_p/(c_p-R)$, we get $\gamma = 1.402$

There are several points to observe regarding (5.1). The last terms of the momentum and energy equations (involving derivatives of u with regard to y) would not be present for strictly one-dimensional flow. However, it may be possible in some situations to make realistic assumptions regarding the u-profile which would allow reasonable approximations to these terms to be included in the solution. In the BLAZE-II program, this is done for the term in momentum equation (but not the dissipation term in the energy equation). No use of these terms is made in the present study. They are included only for completeness. In the absence of the second derivative terms ($\partial^2u/\partial x^2$ in the momentum equation and $\partial^2T/\partial x^2$ in the energy equation) system (5.1) is hyperbolic. Inclusion of either of these second derivative terms makes the system parabolic. If $\partial^2u/\partial x^2$ is omitted from the momentum equation, it is probably inconsistent to retain the dissipation term $(\partial u/\partial x)^2$ in the energy equation. In (5.1), the gas law is used in its original form, rather than using it to eliminate one of the thermodynamic variables as is often done. This approach is used partially for simplicity of formulation and partially to illustrate the flexibility of GEARIB in treating general differential-algebraic systems.

C. Steady Gas Flow Problems

Perhaps the simplest gas flow problems to test GEARIB on are steady flow problems. If all time derivatives are set to zero, (5.1) becomes a system of ordinary differential equations governing steady one-dimensional gas flow. Further, if the axial diffusion terms, $\partial^2u/\partial x^2$ and $\partial^2T/\partial x^2$, are dropped (5.1) can be solved as an initial value problem, i.e., if the state of the flow is specified at any station the solution can be continued downstream in a step-by-step manner. To do this, first rearrange (5.1) dropping all time derivatives and axial diffusion terms and moving the remaining x-derivatives to the LHS. (To be consistent with the omission of $\partial^2u/\partial x^2$, $(\partial u/\partial x)^2$ is also dropped from the energy equation.) Further, but not necessary, assumptions are that the $\partial u/\partial y$ terms in the momentum and energy equations are not present and that $H = H_M$. With this the steady flow specialization of (5.1) is:

$$\begin{bmatrix} u & \rho & 0 & 0 \\ 0 & \rho u & 1 & 0 \\ 0 & 0 & -u & \rho u c_p \\ 0 & 0 & 0 & 0 \end{bmatrix} \begin{Bmatrix} d\rho/dx \\ du/dx \\ dp/dx \\ dT/dx \end{Bmatrix} = \begin{Bmatrix} [M - \rho u \frac{dA}{dx}]/A \\ -(u-u_M)M/A + \rho F + F_N/A \\ Q/A - \frac{u}{A}[(u_M-u)M + F_N] \\ p - \rho RT \end{Bmatrix} \tag{5.2}$$

Now with ρ, u, p, and T specified at any station (ρ, p, and T must satisfy the gas law) (5.2) can be integrated to obtain the solution downstream. It is quite possible that for arbitrary initial conditions and forms of M, A, F, F_N, and Q that no solution will exist. This becomes apparent during the integration when the Mach number approaches unity and the derivatives grow unboundedly. Such problems are always terminated by error conditions internal to GEARIB. Even in those problems for which passage through Mach one is legitimate, e.g., at the throat of a Laval nozzle, attempts to solve by the initial value approach are at best risky even if the upstream conditions are known, which is usually not the case.

A variety of steady flow cases were attempted. No case was run with the body force term, ρF, present in (5.2). However, each of the other terms on the RHS of (5.2) were present in at least some of these tests. For many of the test cases, exact solutions are available.

In the first set of tests, the area was prescribed to be:

$$A(x) = 1 + K(1-x)^2, \tag{5.3}$$

where K is a positive constant. (5.3) is a convergent-divergent duct with its throat at x=1. The integrations all began at x=0 using several different initial conditions, both subsonic and supersonic. The integration proceeded rapidly except in those cases where the flow choked, i.e., reached Mach one before the throat. For such choked flows, often many small integration steps were taken in the neighborhood of Mach one before GEARIB concluded that the step size was unacceptably small.

The next set of tests was for a constant area duct with non-zero wall friction, i.e.,

$$F_N = -K\rho u^2, \tag{5.4}$$

where K is a positive constant. This form for F_N was taken from p. 60 of Oswatitsch [19], who also provides a corresponding exact solution. Different

initial conditions, both subsonic and supersonic, and different values of K were tested. For a long enough duct, the flow will approach Mach one from either a supersonic or subsonic initial state. The larger the value of K the more quickly Mach one will be reached. This was borne out by the numerical results which agreed well with the exact solution of Oswatitsch. For those cases for which Mach one was approached before the end of the duct, the integration broke down just as in the case of choked flow in a convergent-divergent duct.

The next set of tests were run with constant heat addition (Q = constant) in a constant area duct. Again, there are exact solutions for this problem, Oswatitsch [19], p. 68. The effect of heat addition is similar to that of wall friction in that the flow tends toward Mach one regardless of whether the initial conditions were subsonic or supersonic. This was observed in the numerical tests. Agreement with the exact solution was good.

Another set of tests was run with a constant rate of mass addition (M = constant), with $H_M = H$ and $u_M = 0$. The effect of mass addition is similar to that of friction and heat addition, i.e., to always drive the flow toward Mach one. This was observed in the numerical tests but we had no exact solutions for a precise comparison of numerical results.

The final steady flow tests were with a convergent-divergent duct; the cross-section again being given by (5.3). This time, however, the integration was started from the throat (x=1.) with sonic conditions. The difficulty with this problem is that specification of the four dependent variables at the throat is not enough to uniquely determine the solution when the flow is sonic there. This can be seen as follows: differentiate the last equation of (5.2) with respect to x and move it to the LHS. It is possible to solve for the derivative vector only if this modified matrix on the left does not have a vanishing determinant. It is straightforward to evaluate this determinant to be,

$$\det = \rho^2 u[(R-c_p)u^2 + Rc_pT] \tag{5.5}$$

Using the relations $R = (c_p - c_v)$ and $c^2 = (\gamma-1)c_pT$ (c is the speed of sound), it can be seen that the determinant vanishes when $u=c$. In this case, it is possible to obtain solutions for the derivative vector only if the RHS of the modified form of (5.2) vanishes, which it does for the case currently under consideration. Now if one of the derivatives is specified, it is possible to solve for the other three from (5.2). However, this first derivative cannot be selected arbitrarily. Oswatitsch [19], p. 52 shows how to obtain du/dx at the throat by evaluating an indeterminate form. The result is

$$\frac{du}{dx} = \pm \frac{c}{A}\sqrt{\frac{A}{(\gamma+1)}\frac{d^2A}{dx^2}}, \tag{5.6}$$

where the plus sign corresponds to supersonic flow in the expanding section of the duct, the minus sign corresponds to subsonic, and c is again the speed of sound. Since the A we have been considering is in analytical form (5.3), it is easy to use (5.6) to get du/dx and then (5.2) to get the other derivatives.

Why are these considerations important? Suppose one attempted to start the GEARIB integration by selecting the initial derivatives arbitrarily and taking a very small initial step. Even if this were successful, it would be a matter of chance which branch of the solution (supersonic or subsonic) were followed. However, there is doubt whether the integration would get started at all. The Newton matrix (computed by GEARIB) becomes singular at the throat for the same reason the derivative matrix is singular. For a very small initial step (necessary because of the arbitrarily selected initial derivatives), the Newton matrix is nearly singular and the Newton iterations may not converge, which means that the integration cannot get started at all.

By using formulas (5.6) and (5.3) to compute the correct values of the initial derivatives, it was possible to take a moderate sized initial step along either the subsonic or supersonic branch and the integration proceeded without difficulty.

D. Hyperbolic Unsteady One-Dimensional Gas Flow Problems

As noted previously in this section, if the axial diffusion terms, $\partial^2 u/\partial x^2$ and $\partial^2 T/\partial x^2$, in (5.1) are omitted the gas flow problem becomes hyperbolic. For such gas flow problems, there is an extensive literature applying to both the analytical side of the problem, e.g., Courant and Friedrichs [20], and to its numerical aspects, e.g., Richtmyer and Morton [11]. The great majority of numerical methods in use for these hyperbolic problems employ methods which are effectively explicit for the marching (in time) phase of the solution. Explicit marching is generally satisfactory since these hyperbolic systems are usually not stiff. However, if axial diffusion terms are present, the system becomes parabolic and possibly stiff (depending on the magnitude of the diffusion coefficients) and explicit marching methods may be inefficient. (Flows containing axial diffusion effects are considered in Section V.E.) Even more important than axial diffusion from the standpoint of laser simulations is the presence of chemical reactions. Generalization of (5.1) to include finite rate chemistry would render the system very stiff (but still hyperbolic) and the use of implicit marching methods are practically mandatory. It is with a view to the future treatment of reacting gas flows that we have concentrated our attention on implicit integration methods (as in GEARIB).

The spatial differencing scheme used to reduce (5.1) to a system of ordinary differential equations is again the box scheme, i.e., each of the PDE's is written at the midpoint of each mesh interval by approximating each term of the PDE in terms of quantities (dependent variables and prescribed functions) corresponding to the endpoints of the mesh interval. Just as with Burger's equation (discussed in Section IV.C) mesh nonuniformity does not complicate this spatial differencing process.

One question of crucial importance regarding system (5.1) and its spatially discretized counterpart is the question of the allocation of boundary conditions. Since we are not considering axial diffusion terms presently, system (5.1) contains only first derivative terms with respect to x, and so we expect that it will be necessary to prescribe three boundary conditions. In the case of strictly supersonic flow, no downstream information can be propagated upstream. Consequently, no downstream boundary condition can have any effect on the flow, and so all three boundary conditions are imposed at the upstream boundary. On the other hand, for strictly subsonic flow, a characteristic analysis of (5.1) (omitting, of course, $\partial^2 u/\partial x^2$ and $\partial^2 T/\partial x^2$) shows that one of the three characteristic directions runs upstream, which leads to the conclusion that two boundary conditions should be imposed upstream and one downstream. In (5.7), the spatially discretized form of (5.1) is shown for subsonic flow.

As before, H_i is the width of the ith mesh interval. In forming (5.7) from (5.1), terms containing the viscous effects have been dropped in addition to $\partial^2 u/\partial x^2$. the body force term F has been omitted, and it has been assumed that $u_M = u$ and $H_M = H$, which results in the disappearance of other terms. These assumptions are not necessary but have been used for all the numerical tests during this study. Before forming (5.7), we have (for simplicity) replaced $(\rho \partial u/\partial x + u \partial \rho/\partial x)$ by $\partial(\rho u)/\partial x$ in the continuity equation and $u\, \partial u/\partial x$ by $1/2 \partial(u^2)/\partial x$ in the momentum equation. There are other terms in (5.7) which could have been approximated in another way with equal order of accuracy, i.e., it is often a question of whether to replace a product term from (5.1) by the average of the product or the product of the average. Further, if a function is prescribed continuously, it may be simpler to replace an average by its known mid-interval value, e.g., $(M_1 + M_2)/(A_1 + A_2)$ from the continuity equation (written for the first mesh interval) could instead be $M_{1/2}/A_{1/2}$. The decision how to handle such terms is usually a matter of convenience and efficiency, since comparable accuracy is attained with any of the various forms.

In (5.7) g_1, g_2, and g_N are the boundary condition functions. As shown they are quite general. In most of our tests they are usually specialized to a condition that a dependent variable at the end take on a prescribed constant or sometimes a time dependent function. However, for one example, the downstream boundary condition (at the throat of a convergent duct) was that the flow become sonic at a certain time. In this case, the function g_N of (5.7) was a nonlinear function of u_N, T_N, and t. As noted previously, for strictly supersonic flow, all boundary conditions must be imposed at the upstream end, which means that the last equation of (5.7) should be moved to the third row and all the others (except the first and second) should be shifted down. The problem of mixed supersonic-subsonic flows is much more complicated, and will not be considered here. However, in Section V.E it will be shown how such problems can be treated by the introduction of viscosity, which converts the hyperbolic problem to a parabolic problem. Also, in the second year of this study, the supersonic-subsonic problem will be examined using a purely hyperbolic system of governing partial differential equations.

$$
\begin{bmatrix}
0 & 0 & 0 & 0 & 0 & 0 & 0 & 0 & & & & & & & & \\
0 & 0 & 0 & 0 & 0 & 0 & 0 & 0 & & & & & & & & \\
0 & 0 & 0 & 0 & 0 & 0 & 0 & 0 & & & & & & & & \\
.5 & 0 & 0 & 0 & .5 & 0 & 0 & 0 & & & & & & & & \\
0 & .5 & 0 & 0 & 0 & .5 & 0 & 0 & & & & & & & & \\
0 & 0 & \frac{-.5}{c_p\rho_1} & .5 & 0 & 0 & \frac{-.5}{c_p\rho_2} & .5 & & & & & & & & \\
 & & & & & & & & \ddots & & & & & & & \\
 & & & & & & & & .5 & 0 & 0 & 0 & .5 & 0 & 0 & 0 \\
 & & & & & & & & 0 & .5 & 0 & 0 & 0 & .5 & 0 & 0 \\
 & & & & & & & & 0 & 0 & \frac{-.5}{c_p\rho_{N-1}} & .5 & 0 & 0 & \frac{-.5}{c_p\rho_N} & .5 \\
 & & & & & & & & 0 & 0 & 0 & 0 & 0 & 0 & 0 & 0 \\
 & & & & & & & & 0 & 0 & 0 & 0 & 0 & 0 & 0 & 0
\end{bmatrix}
\begin{Bmatrix}
\dot{\rho}_1 \\ \dot{u}_1 \\ \dot{p}_1 \\ \dot{T}_1 \\ \dot{\rho}_2 \\ \dot{u}_2 \\ \dot{p}_2 \\ \dot{T}_2 \\ \cdot \\ \cdot \\ \cdot \\ \cdot \\ \dot{\rho}_{N-1} \\ \dot{u}_{N-1} \\ \dot{p}_{N-1} \\ \dot{T}_{N-1} \\ \dot{\rho}_N \\ \dot{u}_N \\ \dot{p}_N \\ \dot{T}_N
\end{Bmatrix}
=
\begin{Bmatrix}
g_1(\rho_1,u_1,p_1,T_1,t) \\
g_2(\rho_1,u_1,p_1,T_1,t) \\
p_1 - \rho_1 R T_1 \\
\left[(M_1 + M_2) - (\rho_1 u_1 \frac{\partial A_1}{\partial x} + \rho_2 u_2 \frac{\partial A_2}{\partial x}) - (\rho_1 \dot{A}_1 + \rho_2 \dot{A}_2)\right]/(A_1 + A_2) - (\rho_2 u_2 - \rho_1 u_1)/H_1 \\
- (u_2^2 - u_1^2)/2H_1 - (1/\rho_1 + 1/\rho_2)(p_2 - p_1)/2H_1 + (F_{N1} + F_{N2})/(\rho_1 A_1 + \rho_2 A_2) \\
- (u_1 + u_2)(T_2 - T_1)/2H_1 + \frac{1}{c_p}(u_1/\rho_1 + u_2/\rho_2)(p_2 - p_1)/2H_1 + \frac{1}{2c_p}(Q_1/\rho_1 A_1 + Q_2/\rho_2 A_2) \\
+ \frac{1}{2c_p}(u_1 F_{N1}/\rho_1 A_1 + u_2 F_{N2}/\rho_2 A_2) \\
\cdot \\ \cdot \\ \cdot \\ \cdot \\ \cdot \\ \cdot \\ \cdot \\ \cdot \\ \cdot \\ \cdot \\ \cdot \\
p_N - \rho_N R T_N \\
g_N(\rho_N,u_N,p_N,T_N,t)
\end{Bmatrix}
\tag{5.7}
$$

All of the test cases run with system (5.7) used a uniform mesh and the total number of mesh points was 25, making a total of 100 problem unknowns. The first set of tests was for strictly supersonic flow in a constant area duct. The problem was made unsteady by superposing a sinusoidal velocity perturbation on the uniform velocity that would occur in steady flow for the prescribed boundary conditions. Perturbations of several magnitudes, but all satisfying the velocity boundary conditions, were used. Because the flow was supersonic, the perturbations eventually disappeared out of the downstream end of the duct and uniform flow, consistent with the upstream boundary conditions, was realized.

Next a similar set of tests was run with a convergent duct. The initial conditions were obtained by integrating the steady state equations (5.2) subject to the prescribed upstream boundary conditions using GEARIB. A sinusoidal velocity perturbation was superposed on this steady state velocity profile. Again the perturbation eventually passed out of the downstream end of the duct and the steady state solution was assumed (to within the accuracy of the spatial discretization of (5.7)).

For the next test (still strictly supersonic), the initial condition was uniform flow in a constant area duct. The area function was then varied smoothly in time ($0 \leq t \leq 1$) to a convergent duct. Shortly after t=1, the expected steady state solution appeared (to within the spatial discretization error).

The next set of tests was for strictly supersonic flow in a constant area duct. Three tests were made. In all cases, the initial condition was uniform flow. For the first test uniform heat addition was introduced for t>0. For the second uniform mass addition was introduced for t>0. For the third wall friction was specified for t>0 according to the formula (5.4). In none of these tests was the strength of the heat or mass addition or the friction great enough to cause Mach one to be reached before the end of the duct. In all cases, the integration proceeded smoothly and the expected steady state solution (obtained by integrating the steady flow equations (5.2)) was obtained.

The remaining tests were made for strictly subsonic flow. Recall that one boundary condition is now imposed at the downstream end of the duct. If all boundary conditions were prescribed arbitrarily, it would be more difficult to obtain a steady state check case since the steady state equations (5.2) would have to be solved as a two-point boundary value problem instead of as an initial value problem. To avoid this, a steady state subsonic flow was obtained by prescribing three upstream conditions and then integrating (5.2) downstream. The downstream boundary condition for the unsteady problem was then obtained from this steady flow solution. (Of course, one of the three upstream conditions would be discarded.)

For the first test case, the initial condition was uniform flow in a constant area duct. The two upstream conditions were constant values of pressure and density. Uniform mass addition was introduced for t>0. Also, for t>0 the downstream pressure began to vary smoothly from its uniform flow value to the known steady flow value (as explained in the preceding paragraph). Because the flow is subsonic, it takes longer than the analogous supersonic case for a steady state to be reached. Eventually, it was reached with the expected accuracy.

For the next case, the initial condition was steady flow in a convergent duct with a throat at the downstream end. p_1 and ρ_1 were prescribed to be constant at the upstream end. At the throat, u_N was specified to make a smooth transition in time from its initial condition value to sonic value at t = .005. The sonic condition can be written,

$$u_N = \sqrt{(\gamma-1)c_p T_N} \tag{5.8}$$

The integration went smoothly as GEARIB had no difficulty handling this boundary condition. There was no steady steady check, but the solution did seem plausible and sonic conditions were realized at the throat to at least nine significant figures.

For the final test, an attempt was made to solve a subsonic flow problem in a convergent-divergent duct having sonic conditions at the throat. Unlike the problem described in the preceding paragraph, the boundary condition to be applied at the downstream end in order to obtain sonic conditions at the throat is unknown. The approach taken was this. The steady state equations were integrated downstream from the throat taking the initial conditions for this integration from the solution of the preceding problem. The downstream pressure boundary condition for the unsteady problem was then obtained from this solution to the steady state equations.

The initial condition for the unsteady problem was a strictly subsonic flow obtained by integrating the steady flow equations subject to the prescribed values of ρ_1 and p_1 and to a value of u_1 less than that which would produce sonic conditions at the throat. With this initial condition, p_N was varied smoothly in time from its initial condition to the value which should produce sonic conditions at the throat. The integration proceeded smoothly until well after p_N had reached its final value. The solution had almost reached steady state when the velocity became slightly supersonic at the throat. After that the numerical solution began to blow-up. Once the flowfield becomes partially subsonic and partially supersonic, it is not surprising that this should occur since the numerical technique being used is not designed to handle such situations. Why the solution became supersonic in the first place is not clear. It could easily be due to a truncation error in the numerical solution. It might also be a true physical effect. In any case, this test demonstrates the perils of attempting to solve mixed subsonic-supersonic flows using straightforward methods.

E. Parabolic Unsteady One-Dimensional Gas Flow Problems

In this section, we consider several gas flow problems for which an axial diffusion term is present in the governing system (5.1). The diffusion term included is $\partial^2 u/\partial x^2$ from the momentum equation. (To be consistent $(\partial u/\partial x)^2$ is also retained in the energy equation.) The $\partial^2 T/\partial x^2$ term from the energy equation could have been retained instead, or in addition to, $\partial^2 u/\partial x^2$. However, for simplicity it was decided to keep only one of these diffusion terms. If only one is to be kept then it probably should be $\partial^2 u/\partial x^2$ since viscosity has a more important influence on the effects we hope to observe, i.e., the transition from supersonic

to subsonic flow, than does heat conduction. See Richtmyer and Morton [11], p. 311 ff. for some discussion of this point. Even when both viscous and heat conduction effects are included it is known that the corresponding solutions cannot be valid within shocks, since the continuum assumption is not a good approximation in such narrow regions of rapid transition. See von Mises [18], p. 142 ff., Oswatitsch [19], p. 550, and Courant-Friedrichs [20], p. 137 for discussion. Despite this shortcoming, the inclusion of viscous effects is at least a convenient numerical device to make downstream changes have an effect upstream in supersonic flow and to obtain the transition from supersonic to subsonic flow, and at best also gives a good approximation to reality outside the shock.

To maintain the convenience and flexibility of the box method, the $\partial^2 u/\partial x^2$ term cannot be replaced by a 3-point divided difference formula and then be inserted into the appropriate equations of the differential system (5.7). Instead the device already employed in the treatment of Burger's equation is used, i.e., define

$$v \equiv \frac{\partial u}{\partial x} \tag{5.9}$$

Now replace $\partial u/\partial x$ by v and $\partial^2 u/\partial x^2$ by $\partial v/\partial x$ on the RHS of (5.1), and approximate the partial differential equations at the mid-point of each mesh interval just as was done to obtain (5.7). Of course, there is now an additional dependent variable, v_i, at each node and for each interval an additional equation, the discretized form of (5.9),

$$0 = (v_i + v_{i+1})/2 - (u_{i+1} - u_i)/H_i \tag{5.10}$$

To obtain a tight band structure for the Newton matrix that is computed by GEARIB, v_i is inserted between u_i and p_i in the dependent variable vector of (5.7), and (5.10) is inserted between the continuity and momentum equations of (5.7) (written for the i-th interval).

In going from (5.7) to the augmented system containing the effects of viscosity, N unknowns (the v_i) have been added but only N-1 new equations ((5.10) for each of the N-1 intervals) have been written. Because of the presence of the 2nd derivative term, $\partial^2 u/\partial x^2$, in the governing partial differential system (5.1), we expect that an additional boundary condition will be required. The only question is whether this boundary condition should be applied at the upstream or downstream boundary. Initially, a variety of simple problems were attempted with two boundary conditions imposed upstream and two downstream. All of these attempts failed, the computed solution growing unbounded or at least continuing to deviate from its known steady state solution. This occurred with both purely supersonic and purely subsonic initial conditions which were only slight perturbations of the known steady state solution, and with a variety of combinations of boundary conditions. Based on these numerical experiments, it was concluded that for the problem to be properly posed, it is necessary to impose three boundary conditions upstream and one downstream regardless of whether the flow is supersonic, subsonic, or mixed. There appears to be very little guidance in the literature as to the appropriate boundary conditions

for one-dimensional gas flow with viscosity. For example, Benison and Rubin [21] solve such problems for ducts of variable cross section (including also the effects of thermal conductivity) by explicit marching methods. If one is not interested in details of the flow near the ends of the duct, e.g., if the ends are in regions of uniform flow, then it is possible to be rather loose about the specification of boundary conditions if implicit methods are being used. Benison and Rubin effectively overspecify the number of boundary conditions in order to facilitate the use of their explicit method. When using some implicit methods with purely hyperbolic problems such an overspecification of boundary conditions is sometimes necessary. It is a subject of some controversy how seriously this affects the solution within the region of interest. See Mitchell [22], p. 167 ff. for some discussion. Similar difficulties arise when explicit methods are used for hyperbolic problems. See Kreiss [23] for a detailed discussion of this problem. Ludford, Polachek, and Seeger [24] and Moretti and Salas [25] solve one-dimensional viscous flow problems made unsteady by the motion of a piston at one boundary. Both papers use explicit methods. Ludford et. al. deal with the boundary condition question by effectively formulating the problem in Lagrangean variables and using a staggered grid, which requires them to specify only the values of the velocity on the boundaries. Moretti and Salas resort to overspecification of the boundary conditions.

The first unsteady viscous problem attempted was flow in a constant area duct which is initially uniform supersonic. The single downstream boundary condition (usually pressure for our tests) was altered smoothly in time so that the flow near the downstream end would become subsonic. (At the upstream boundary, the flow remained supersonic because of the three boundary conditions imposed which were held constant for our tests.) If the final value of the downstream boundary condition is "just right" then the steady state solution will approach uniform supersonic flow upstream and uniform subsonic flow downstream with a rather rapid transition from supersonic to subsonic somewhere in the interior. The width of this transition decreases with the viscosity and can be thought of as simulating a shock for small viscosity. The corresponding steady flow problem is discussed in detail in von Mises [18], p. 139 ff., who also supplies an exact solution (in implicit form). This exact steady solution was built into our unsteady flow program for two purposes: (1) to supply the downstream boundary condition appropriate to the prescribed upstream conditions so that uniform flow upstream and downstream would be realized as the unsteady solution approached steady conditions, (2) to provide a steady state check for the unsteady solution.

Before actually attempting the problem described in the preceding paragraph, a series of tests were made using as the initial condition a perturbation of the exact steady flow solution (uniform supersonic upstream and uniform subsonic downstream). The single downstream condition was specified in several ways. If ρ_N, u_N, p_N, or T_N were prescribed (equal to their steady flow value), the perturbation died out rapidly, as expected, and the exact steady solution was obtained (to within the truncation error of the spatial discretization). However, when $v_N \left(\equiv \left.\frac{\partial u}{\partial x}\right|_{x_N}\right)$ was prescribed, the solution departed more and more from the steady solution, even for very small initial perturbations. Several further tests were

performed with v prescribed at the downstream boundary. For these tests, the solution was attempted over subintervals of the original x-interval; some tests were for a strictly supersonic interval, some for strictly subsonic, and some for mixed supersonic-subsonic. The initial conditions and boundary conditions were again taken from the exact steady flow solution. Of course, the boundary conditions do not necessarily correspond to uniform flow since only a portion of the original x-interval is being considered. For an x-interval corresponding to strictly supersonic flow, the unsteady solution returned to the exact steady flow solution after an initial perturbation. For an x-interval that was primarily supersonic but with a subsonic portion downstream, the unsteady solution would depart from the initial steady flow solution (even with no perturbation) and it would eventually approach another quite different strictly supersonic steady flow solution, the significance of which was not clear. For strictly subsonic initial conditions, the unsteady solution would depart from the initial conditions with ever increasing spatial gradients and gave no indication that it would eventually reach a steady state. Although the significance of these experiments with v_N prescribed downstream is unclear, it is apparent that it is dangerous to prescribe v to be a boundary condition. Such boundary conditions were not employed in the remainder of our numerical tests.

We now discuss the unsteady viscous flow problem of interest. For this problem, the initial condition was uniform supersonic flow (Mach 1.4). Starting at t=0, the downstream pressure was increased smoothly in time from its uniform flow value to its final value at t=.1. (Recall that this value is taken from the exact steady flow solution having uniform supersonic flow upstream and uniform subsonic flow downstream.) This problem was run for three different values of the viscosity. In Figure 5.1, u-profiles corresponding to the smallest value of the viscosity ($\mu = 14.7$) are plotted for various times. For these numerical tests, the x interval was [0,1] which was divided into 80 equally spaced intervals. There are five unknowns per mesh point making a total of 405 dependent variables that were integrated. In Figure 5.1, the profile labeled "$t=\infty$" is taken from the exact steady flow solution. The last profile actually obtained from the unsteady integration is for $t = 2.4$. Conditions are still slowly changing at $t = 2.4$, but it seems doubtful whether the unsteady integration would ever reach the "$t=\infty$" profile. The reason is that the position of the rapid transition is not well defined, especially for small values of μ. The shape of the profile is well defined, and it can be seen that the $t = 2.4$ and $t=\infty$ profiles are practically translates of each other. For larger values of μ the position is better defined. For numerical tests with $\mu = 23.1$ and $\mu = 34.6$, the unsteady solution came much closer to the exact steady solution. The reason for this type of behavior is that the exact solution attains uniform conditions only at $x = \pm\infty$, and any finite translate of such an exact solution is also an exact solution. For our purposes, we have chosen the exact steady solution which undergoes the rapid transition from supersonic to subsonic near $x = .5$. Now the x derivatives of this solution are finite at x=0 and 1., but they decrease with μ. Thus, for the smaller values of μ, the conditions at x=0 and 1. more closely resemble uniform flow, which means that there is a group of translates of the exact steady flow solution which comes very close to satisfying the equations we are integrating along with the boundary conditions at x=0 and 1.

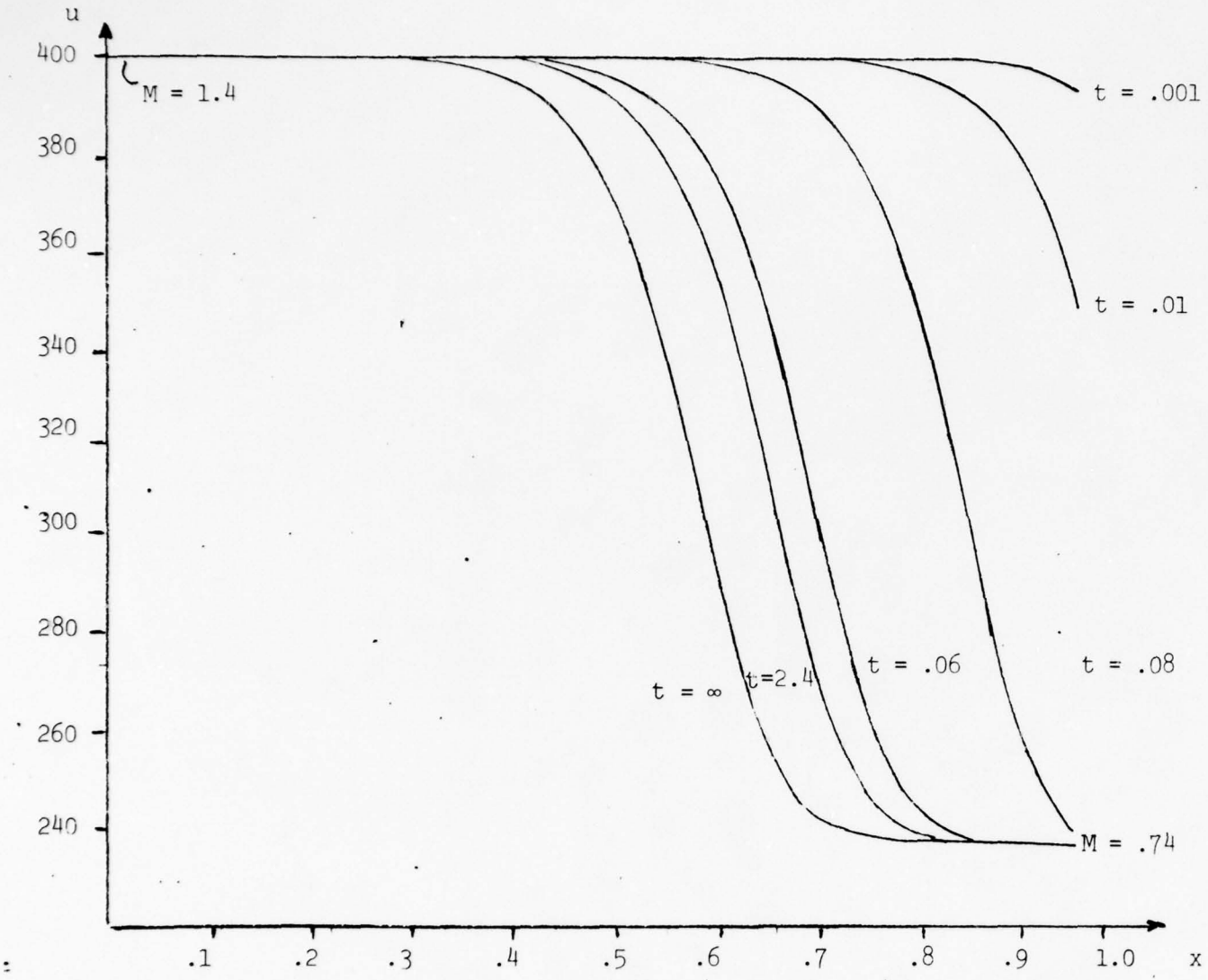

Figure 5.1 u-Profiles for Supersonic-Subsonic Unsteady Viscous Flow

Had we attempted the solution of such a problem in a duct of variable cross-section, e.g., the convergent-divergent duct used by Benison and Rubin [ ], we would expect the position of the rapid transition to be well defined regardless of the value of μ since the limiting inviscid solution, i.e., the shock, must occur at a definite location in order that all boundary conditions be satisfied. For our next group of tests, the flow also takes place in a duct of constant cross section, but for some of these runs a special type of nonuniform heat input distribution (Q in system (5.1)) seemed to force the rapid transition to occur about a more clearly defined position in the duct.

The first of the tests with heat input used a Q which was constant in space but varied smoothly in time starting with Q = 0. at t = 0. The prescribed time dependence of Q was such that 80% of its final "steady" rate occurred by t = .02, and by t = .1. Q was constant for practical purposes. The initial condition was uniform supersonic flow. In addition to the time dependent Q, the downstream pressure, p_N, which increased smoothly from its uniform flow value at t = 0 to its final value at t = .1, contributed to the unsteadiness of the problem. Beyond t = .1, the external "driving forces" ceased to have an unsteadying effect, and the flow proceeded toward its asymptotic steady state. For the first set of tests, the initial condition was uniform supersonic flow and the final value of p_N was the same as that used for the runs without heat addition, i.e., that value which would produce uniform supersonic flow upstream and uniform subsonic flow downstream in the absence of heat addition. Several different values of viscosity and strengths of the heat addition rate were tried. Plotted in Figure 5.2 are u-profiles for a typical case: $\mu = 14.7$ and $Q = 10^7 t^2/(t^2 + 10^{-4})$. Except for the heat addition, this case is identical to that of Figure 5.1. Unlike the case of Figure 5.1, which is very slow to reach its steady state (because it is poorly defined - as discussed earlier), the presence of heat addition causes the steady state to be reached very quickly. Of course, the upstream and downstream steady state flows are no longer uniform. (Uniform flow is not possible in regions of the duct where there is heat addition.) As is clear from Figure 5.2, for steady state the transition from supersonic to subsonic flow is made near the upstream end of the duct. For most of the rest of the duct, the velocity increases nearly linearly, which means that the viscosity has little effect in the momentum equation of system (5.1). Viscosity will have some influence on the energy equation through the dissipation term, but this is rather small. Thus, over most of the duct the flow is very similar to an inviscid flow with heat addition.

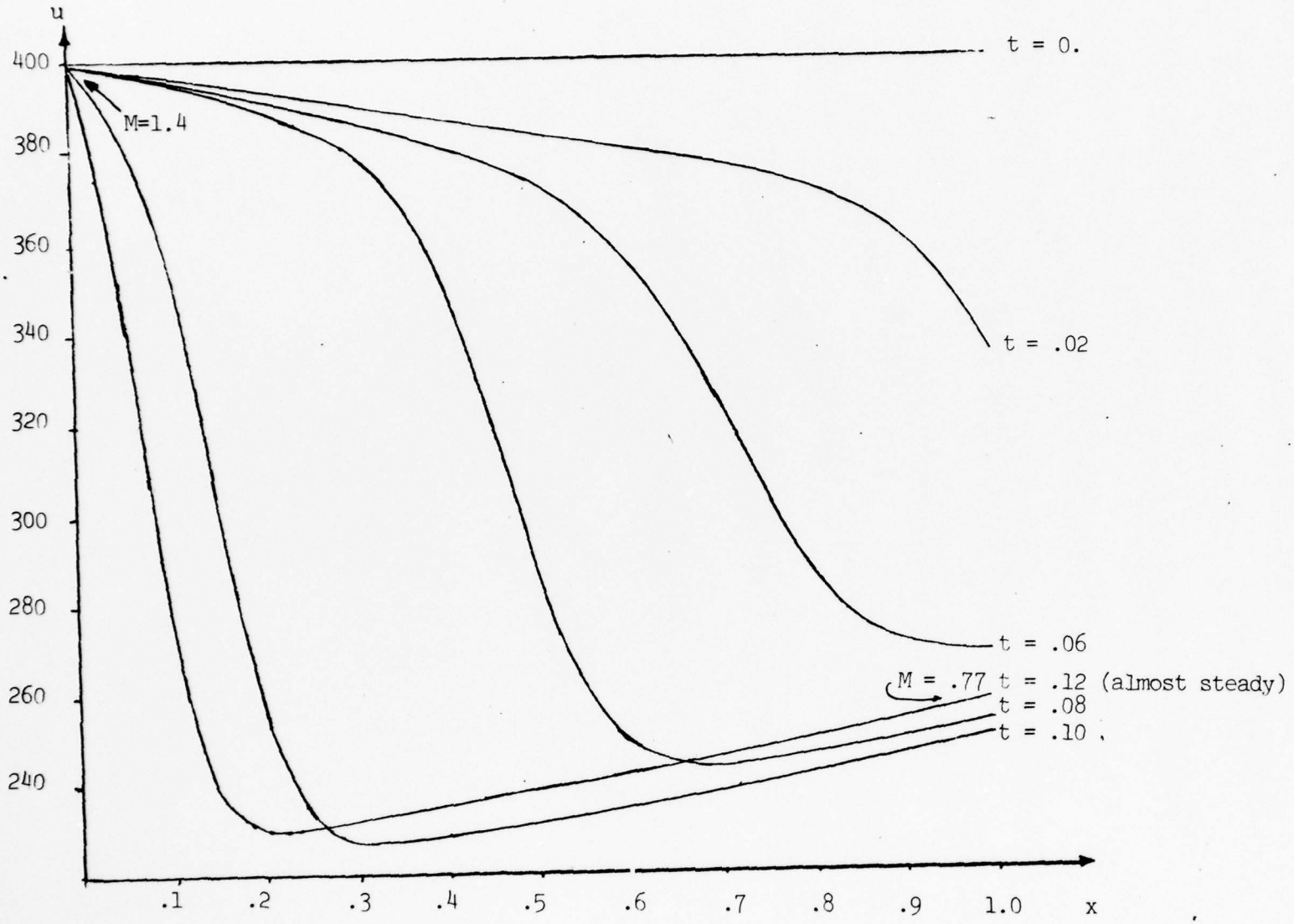

Figure 5.2 u-Profiles for Supersonic-Subsonic Unsteady Viscous Flow with Uniform Heat addition

In order to obtain uniform flow conditions near the ends of the duct and also to ensure a well defined location of the rapid transition through Mach one, the heat addition distribution illustrated in Figure 5.3 was used for the next series of tests.

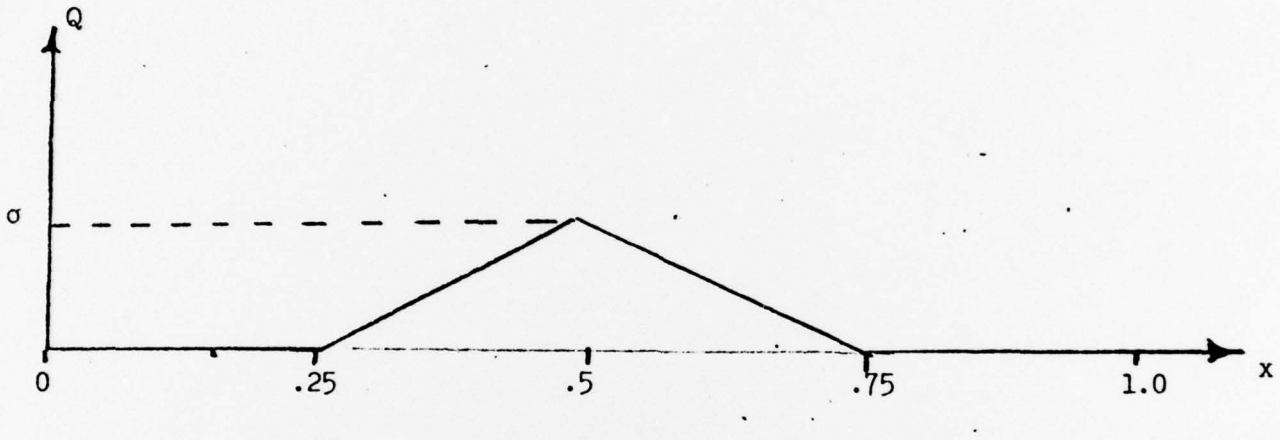

Figure 5.3 Nonuniform Heat Addition Distribution

The Q-profile illustrated represents the steady state heat addition rate. Before Q reaches its steady state value, the distribution in x is similar but with a smaller peak value. The peak value, σ, is chosen to demonstrate particular types of flow features, which are discussed in detail in the following paragraphs.

For inviscid steady flow with heat addition it is possible, for prescribed upstream conditions, to integrate the steady flow equations (5.2) downstream. In this way any continuous steady flow can be obtained. (As discussed in Section V.C, if the heat addition rate is too large, the flow will approach Mach one from either a supersonic or subsonic initial state, at which point the integration will break down, i.e., no continuous solutions exist for the prescribed upstream boundary conditions and heat addition rate.) For constant area ducts, it is not necessary to integrate the steady flow equations numerically. An analytical solution is provided by Oswatitsch [19], p. 68, which requires only that the prescribed Q(x) be integrated, and this is especially easy for the distribution we are using (Figure 5.3). Thus, all continuous solutions to the inviscid steady flow problem with heat addition in a constant area duct are easily obtained.

Corresponding to a uniform upstream flow, there are two possible uniform downstream flows following a section of the duct over which heat is added. One is the continuous solution discussed in the preceding paragraph, which does not pass through Mach one. The other solution contains a shock, i.e., it passes

through Mach one. The position of this shock is arbitrary, which means that it is no longer possible to give details of the flow within the region of heat addition, unless the shock location is somehow specified. There are, however, simple formulas for the uniform downstream flow, Oswatitsch [19], p. 68. For given uniform upstream conditions, these formulas were used to obtain the downstream pressure, p_N, for use as a boundary condition in the viscous flow problem. Just as in the viscous flow problems without heat addition the initial condition was uniform flow, and p_N was varied smoothly from its initial value to this value obtained from the inviscid flow solution. Before giving details of the various viscous flow tests with the heat addition distribution of Figure 5.3, it is useful to discuss the generalized Rankine-Hugoniot curve. This curve is helpful in categorizing the numerical tests that have been made. Additional discussion of this curve can be found in Oswatitsch [19], p. 71 ff. and Courant-Friedrichs [20], p. 210 ff. For a duct of constant cross section with a region of heat addition,

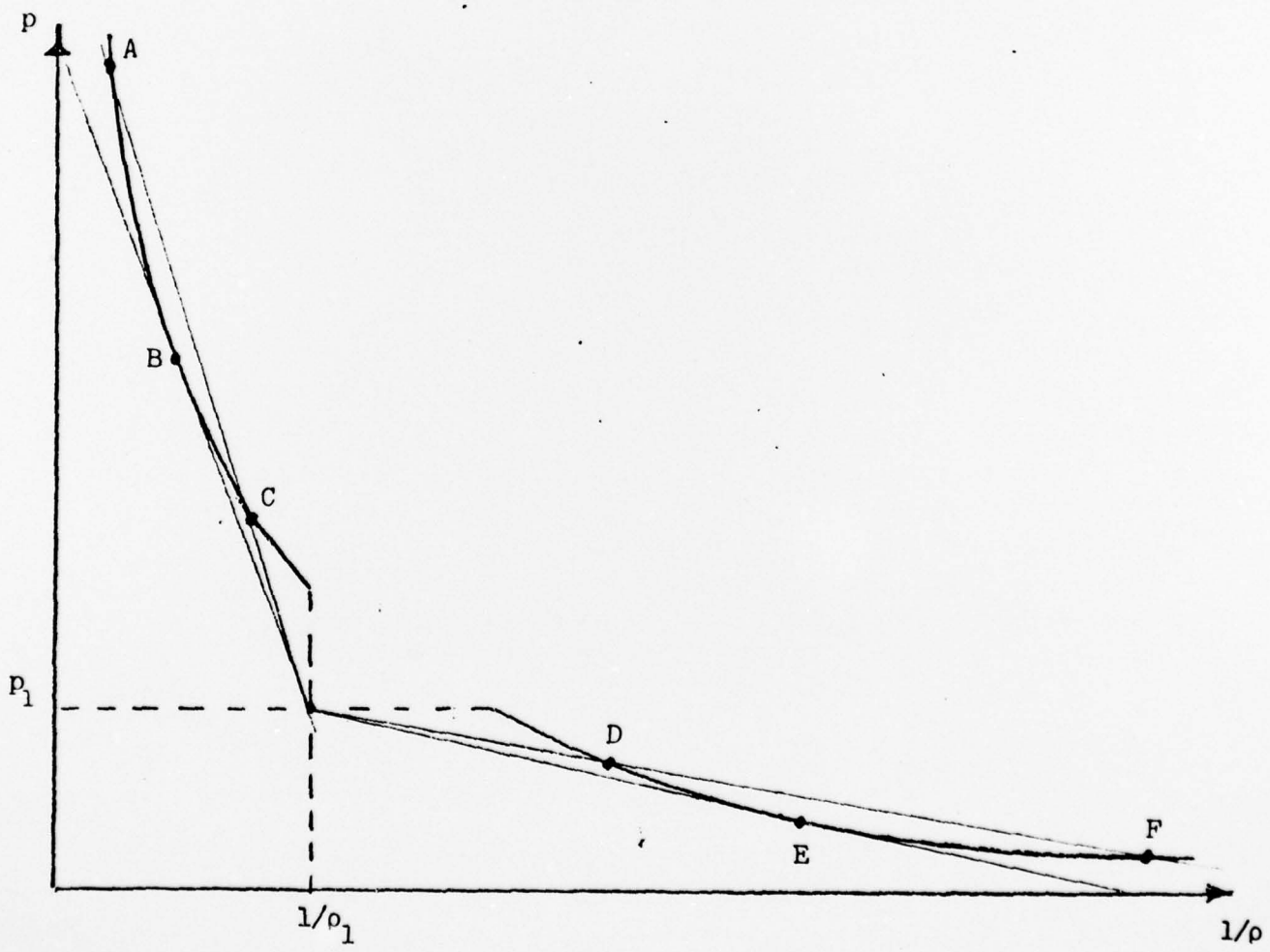

Figure 5.4 Rankine-Hugoniot Curve for Heat Addition

the generalized Rankine-Hugoniot curve shows what downstream densities and pressures (ρ,p) are consistent with the corresponding upstream quantities (ρ_1, p_1). The extent to which the curve is translated from the point $(1/\rho_1, p_1)$ is proportional to the amount added heat per unit mass, i.e., $(1/\rho_1 u_1)\int_{x_1}^{x_N} Q(x)dx$. For no heat addition, the curve would reduce to the usual Rankine-Hugoniot curve and would pass through $(1/\rho_1, p_1)$, i.e., the downstream pressure and density can be identical to the corresponding upstream quantities. Of course, ρ_1 and p_1 do not completely determine the flow; one must specify the upstream velocity, u_1, also. Eliminating the downstream velocity, u, from the continuity and momentum equations (written for the section of the flow extending across the entire region of heat addition) another $(1/\rho, p)$ relation (depending on the prescribed values ρ_1, p_1, and u_1) can be obtained. It turns out that this is a linear relation passing through the point $(1/\rho_1, p_1)$ with a negative slope proportional to $-u_1^2$. This linear relation is plotted in Figure 5.4 for several values of u_1. The intersection points (marked by heavy dots) represent the downstream values of density and pressure that are possible for the given upstream state (u_1, ρ_1, p_1) corresponding to the prescribed heat addition rate. There are either two, one, or no intersection points (depending on u_1). The intersection points to the right of $(1/\rho_1, p_1)$ correspond to subsonic upstream flows and those to the left correspond to supersonic upstream flows. The six intersection points shown in Figure 5.4 can be categorized as follows:

A - supersonic upstream, subsonic downstream (strong detonation)

B - supersonic upstream, sonic downstream (Chapman-Jouguet detonation)

C - supersonic upstream, supersonic downstream (weak detonation)

D - subsonic upstream, subsonic downstream (weak deflagration)

E - subsonic upstream, sonic downstream (Chapman-Jouguet deflagration)

F - subsonic upstream, supersonic downstream (strong deflagration)

For given upstream conditions, the straight line relation of Figure 5.4 is completely determined. Then if the heat addition rate is large enough, the Rankine-Hugoniot curve will be translated far enough from the point $(1/\rho_1, p_1)$ so that there can be no intersection point. This is a geometric illustration of the earlier discussion that a solution may not exist for arbitrary upstream conditions and heat addition rates.

The downstream states corresponding to points B, C, D, and E do not represent passage through Mach one, i.e., they are continuous solutions and could be obtained by integrating the one-dimensional steady flow equations. Point A is a generalization of the usual normal shock, i.e., a discontinuous transition from supersonic to subsonic flow. On the other hand, point F corresponds to a discontinuous transition from subsonic to supersonic flow, i.e., a rarefaction

shock, which, in the absence of heat addition, would violate the second law of thermodynamics. However, if the entropy increase due to heat addition is large enough to compensate for the entropy decrease due to the rarefaction, F could be a legitimate solution.

In our numerical work tests were made corresponding to each of points A, B, C, D, E, and F of Figure 5.4. These six tests were all run for the same Rankine-Hugoniot curve. To accomplish this ρ_1, p_1, and the heat addition rate per unit mass were identical for all runs. Then to obtain the various cases, u_1, was varied and the corresponding downstream pressure was computed from the inviscid solution and used as the downstream boundary condition, p_N, in the viscous solution. (Note that it is necessary to vary $Q(x)$ proportionally to u_1 to maintain the same heat addition rate per unit mass.) In all cases, the initial condition was uniform flow and the heat addition rate and p_N were varied smoothly in time so that their steady values would be attained by $t = .1$ (exactly for p_N, approximately for the heat addition). Unless otherwise noted, all cases were run with $\mu = 14.7$ and 40 equal mesh intervals between $x = 0.$ and $x = 1.$ Thus, there are 205 unknowns to be determined at each step of the integration.

Plotted in Figure 5.5 are velocity profiles for various times for the case of Chapman-Jouguet detonation, point B on the Rankine-Hugoniot curve of Figure 5.4. At steady state, the flow is uniform both upstream and downstream. Also plotted is the steady inviscid solution computed from the formulas of Oswatitsch, which illustrates the effect of viscosity. Similar runs were also made for strong and weak detonations, points A can C on the Rankine-Hugoniot curve. The results had the same character as those of Figure 5.5 and so have not been plotted. Perhaps the most important distinction among the three cases was the time required to reach steady conditions. The strong detonation case took by far the longest time with Chapman-Jouguet detonation next.

In Figure 5.6 are plotted u-profiles for various values of t and also the steady state temperature profile for Chapman-Jouguet deflagration, point E of Figure 5.4. At steady state the downstream flow conditions are not uniform, and there is also a small jump at the upstream end. However, the values of ρ_N, u_N, p_N, and T_N agree with their inviscid counterparts to at least three figures. The total entropy change (which depends only on ρ_1, p_1, ρ_N, and p_N) differs by less than 1% from the corresponding inviscid change. Although viscous dissipation contributes to the entropy increase, it can be seen from Figure 5.6 that the heat is added at a higher temperature in the viscous case. This means that the entropy increase due to heat addition is less in the viscous case, which partially compensates for the entropy increase due to dissipation. If truly uniform conditions are attained downstream then the viscous entropy change is identical to that of the corresponding inviscid flow. (This was true for the detonation cases discussed in the preceding paragraph.)

In an attempt to obtain uniform flow upstream and downstream for Chapman-Jouguet deflagration several things were tried:

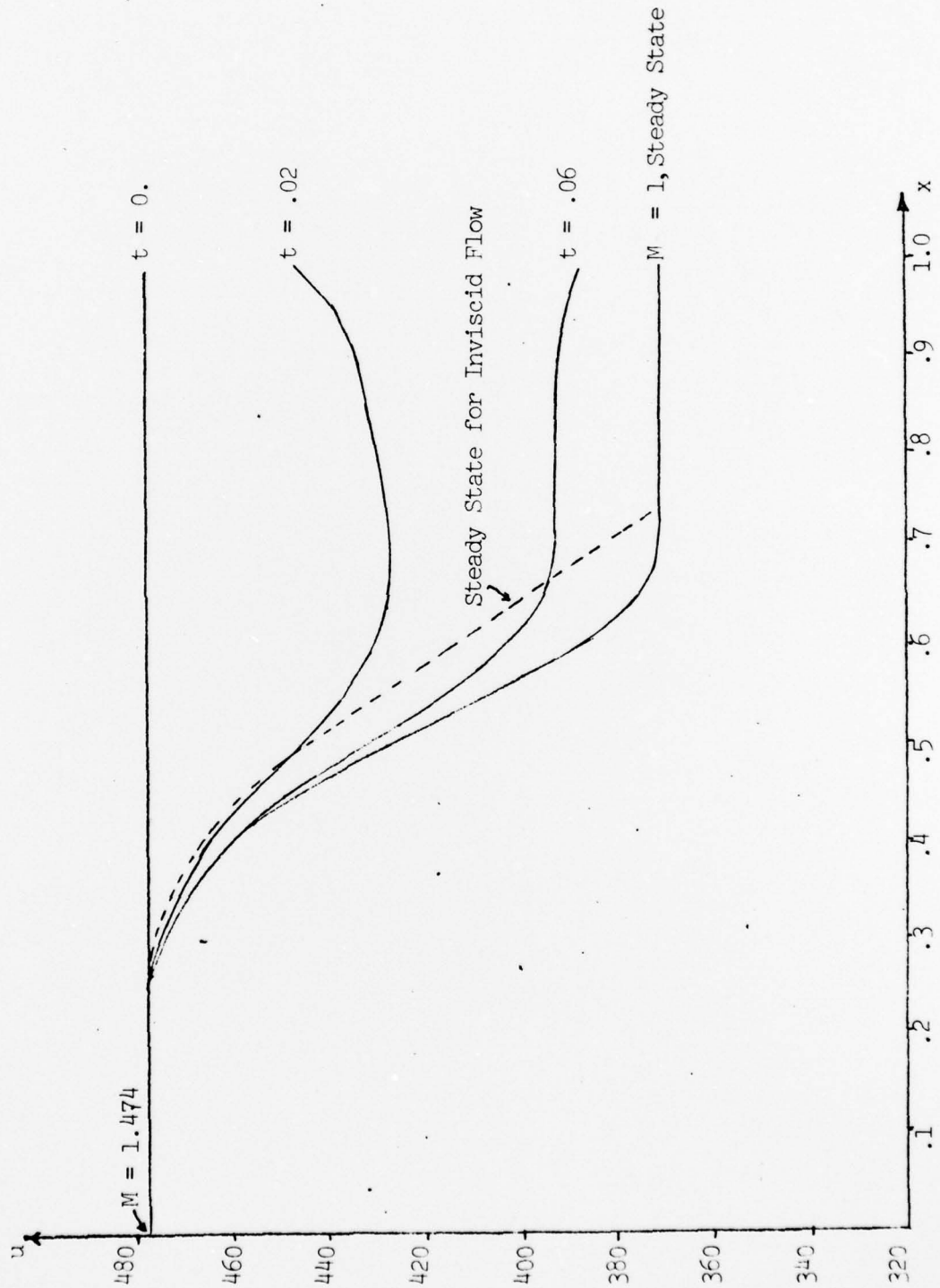

Figure 5.5 u-Profiles for Chapman-Jouguet Detonation

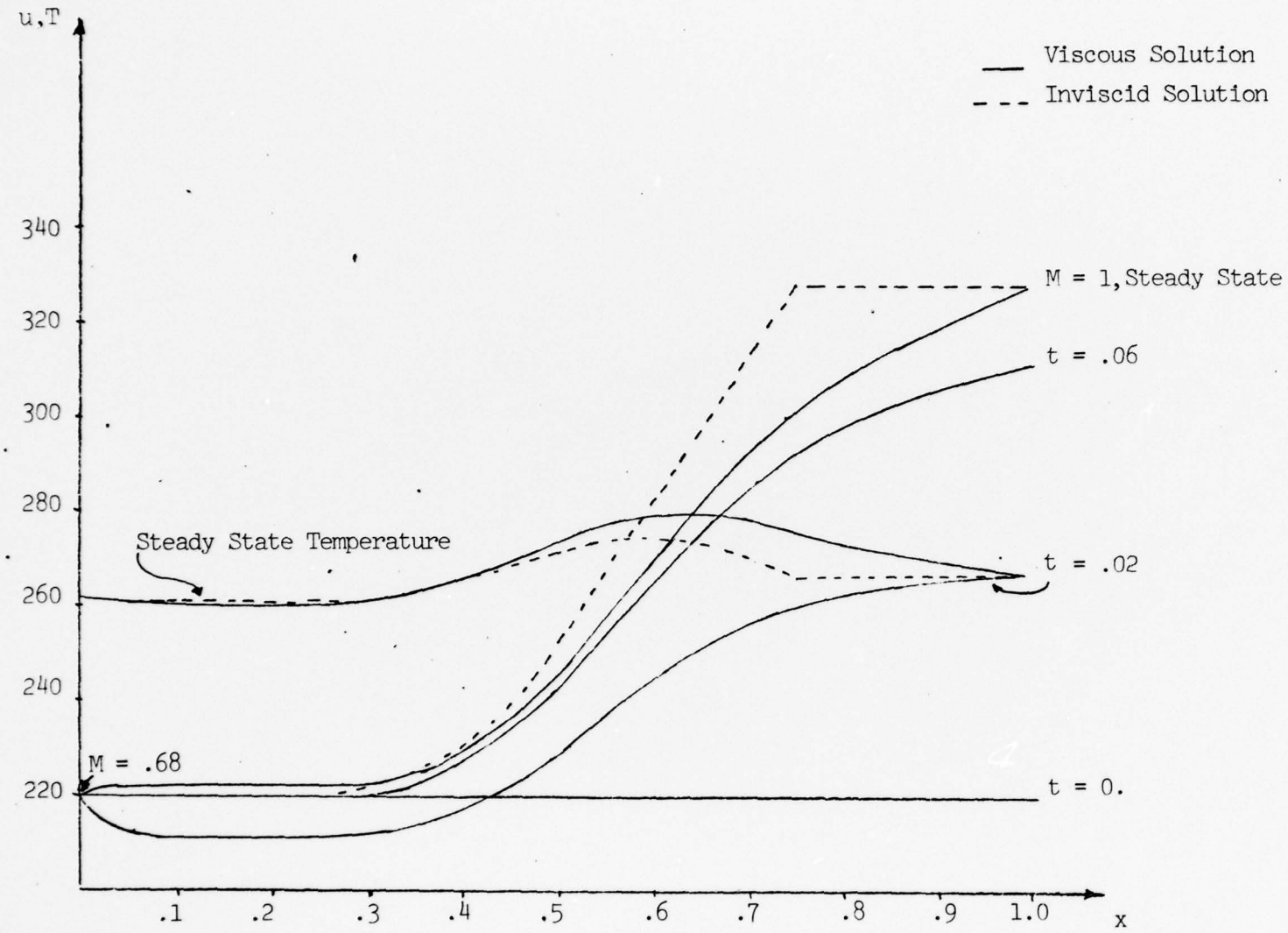

Figure 5.6 u-Profiles and Steady State Temperature for Chapman-Jouguet Deflagration

i) The mesh size was halved (approximately doubling the number of unknowns). This had practically no effect on the solution.

ii) The length of the x-interval was increased to [-.5, 1.5] maintaining the original mesh size. The upstream and downstream flows were closer to being uniform, but still not as good as the detonation cases.

iii) The viscosity was reduced maintaining the original x-interval and mesh size. With $\mu = 1$ (instead of 14.7), steady conditions were more nearly uniform upstream and downstream, but again still not as good as in the detonation cases. The entropy change differed from the inviscid entropy change in the fifth figure. From a numerical standpoint, this case was more difficult than the corresponding $\mu = 14.7$ case. During early stages of the integration, moderately high frequency oscillations, (probably spurious) appeared in the solution, which resulted in GEARIB taking small steps until these oscillations died out.

A test was run for weak deflagration, point D, in Figure 5.4. Uniform flow was attained quite well both upstream and downstream. There are no particular features of this run that are noteworthy, so the results have not been plotted.

The final plot, Figure 5.7, is for strong deflagration, point F in Figure 5.4. It is clear that uniform conditions are not even close to being realized, especially downstream. The steady state values of ρ_N, u_N, and T_N disagreed with the corresponding inviscid values by one or two percent. The total entropy increase was off by about 10%. No attempts were made to obtain uniform upstream and downstream flow by reducing the viscosity or lengthening the x-interval. Based on the numerical work with Chapman-Jouguet deflagration, these "tricks" did not seem promising in view of the more difficult behavior of this problem. Even if there were no numerical problems to overcome, it may be that no amount of viscosity reduction or interval lengthening could produce the desired results. Although the inviscid solution that we were trying to approximate satisfies continuity, momentum, and energy balance plus the second law of thermodynamics, Courant-Friedrichs [20], p. 228 ff., argue that this case is physically impossible, and possibly the unexpected behavior of the viscous solution is a reflection of this fact?

It should be emphasized that in the plots of u-profiles presented in this section, the unsteady profiles are strongly dependent on the rather arbitrary time dependence that was assigned to p_N and the heat addition rate in order to get from their initial values to the steady state values. Other time dependencies could have been selected. In this regard, one precaution should be observed: the time dependencies should be smooth as possible. If there are discontinuities in the time function or its derivatives, GEARIB may have some difficulty in getting past the discontinuity, especially if it is operating with a high order method at the time it encounters the discontinuity. For example, the prescribed time dependency of p_N had a discontinuity in its second derivative at $t = .1$ (the point at which p_N reached its steady state value). Even this mild discontinuity caused GEARIB some difficulty. For stronger discontinuities, the proper approach is to integrate right to the point of discontinuity (assuming it is known in advance), and then restart the integration from this point incorporating the discontinuous change. This is readily accomplished within the framework of GEARIB.

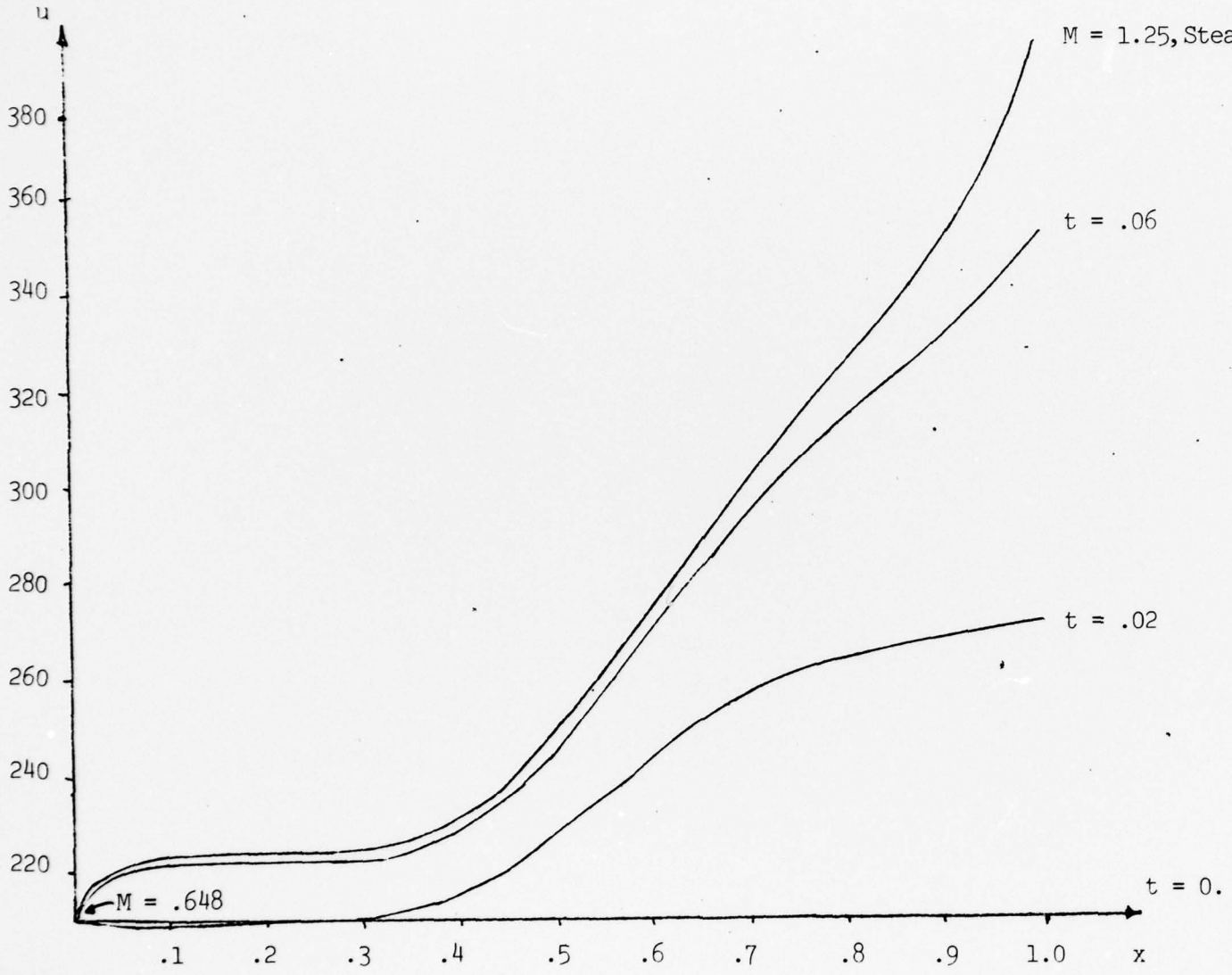

Figure 5.7 u-Profiles for Strong Deflagration

Apart from the discontinuity difficulty discussed in the preceding paragraph, the only other problem with GEARIB was in starting. Recall that in the viscous problem, it was necessary to prescribe three boundary conditions upstream and one downstream. By applying the gas law at mesh point 1, u_1, ρ_1, p_1, and T_1 are fixed (v_1 is free). It turns out that unless v_N is prescribed downstream, the Newton matrix is singular as $h \to 0$. If the algebraic equations of the governing system are differentiated with respect to t and moved to the LHS, then this matrix equation can be solved for the derivative vector only if v_N is prescribed. As noted early in this subsection, it was not possible to obtain reasonable solutions with this downstream boundary condition. Instead for most of our tests p_N was prescribed, leading to a singular derivative matrix and, for small h, a poorly conditioned Newton matrix. This same problem arose in our treatment of Burger's equation in Section IV.C.1, and a detailed analysis of this situation was given there, including possible remedies. One of which was the selection of initial conditions so that the RHS of the differential system would be consistent with the LHS and a solution for the initial derivatives could be obtained (by a special formula) inspite of the singular matrix on the left. Because of the more complicated system being used for the viscous flow problem, this approach was deemed impractical.

The starting technique actually used was the following: A moderately small initial step size was chosen. GEARIB was modified so that the first ten steps would be performed with this same step size. All error and convergence testing was suppressed for these first ten steps. Also, only one Newton iteration was used per step and the Newton matrix was updated before each iteration. After the tenth step, GEARIB began operating in its accustomed mode. In all cases, this starting technique was successful.

VI. RECOMMENDATIONS

1. Examine the potential in computer time savings by using sparse matrix techniques in conjunction with implicit integration methods to improve the efficiency of three-dimensional parabolic flow calculations.

2. Continue development of the unsteady quasi two-dimensional mixing, reacting, lasing flow equation system.

3. Exercise the unsteady flow analysis to examine laser start transient effects and shock wave formation in low diluent-low pressure laser applications.

VII. REFERENCES

1. Baker, A. J. and Zelazny, S. W., "COMOC: Three-Dimensional Boundary Region Variant - Theoretical Manual and User's Guide," NASA CR-132450, May 1974.

2. Nigro, B. J., "The Derivation of Optimally Stable, 3-Stage, 1-Step Explicit Numerical Integration Methods," Bell Aerospace Textron Report TCTN-1010, 1971.

3. Strang, G. and Fix, G., An Analysis of the Finite Element Method, Prentice-Hall, 1973.

4. Hindmarsh, A. C., "GEARIB: Solution of Implicit Systems of Ordinary Differential Equations with Banded Jacobian" (Preliminary Documentation), UCID-30130, Lawrence Livermore Laboratory, February 1976.

5. Curtiss, C. F. and Hirschfelder, J. O., "Integration of Stiff Equations," Proc. Nat. Acad. Science, U.S., Vol. 38, 1952, pp. 235-243.

6. Gear, C. W., "The Automatic Integration of Ordinary Differential Equations," Communications of the ACM, Vol. 14, 1971, pp. 176-179; 185-190.

7. Schlichting, H., Boundary Layer Theory, 4th Ed., McGraw-Hill, 1960.

8. Gross, R. W. F. and Bott, J. F., Handbook of Chemical Lasers, John Wiley and Sons, 1976.

9. Driscoll, R. J., "A Study of the Boundary Layers in Chemical Laser Nozzles," AIAA Journal, Vol. 14, No. 11, November 1976, pp. 1571-1577.

10. Lankford, D. W. and Rapagnani, N. L., "Time Dependent Nozzle and Base Flow/Cavity Model of CW Chemical Laser Flowfields," AIAA Conference on Fluid Dynamics of High Power Lasers, Cambridge, Mass., 31 October - 2 November 1978, Paper IV-3.

11. Richtmyer, R. D. and Morton, K. W., Difference Methods for Initial Value Problems, 2nd Ed., Interscience, 1967.

12. Keller, H. B., "Some Computational Problems in Boundary Layer Flows," Vol. 35, Lecture Notes in Physics; Proceedings of 4th International Conference on Numerical Methods in Fluid Dynamics, Springer-Verlag, 1975, pp. 1-21.

13. Swartz, B. and Wendroff, B., "Generalized Finite-Difference Schemes," Math. Comp., Vol. 23, 1969, pp. 37-50.

14. Sincovec, R. F. and Madsen, N. K., "Software for Nonlinear Partial Differential Equations," ACM Trans. Math. Software, Vol. 1, 1975, pp. 232-260.

15. Cole, J. D., "On a Quasi-Linear Parabolic Equation Occurring in Aerodynamics," Quart. Appl. Math., Vol. 9, 1951, pp. 225-236.

16. Isaacson, E., "Fluid Dynamical Calculations," Numerical Solution of Partial Differential Equations, J. H. Bramble, Ed., Academic Press, 1966, pp. 35-49.

17. Sentman, L. H. Subbiah, M. and Zelazny, S. W. "BLAZE-II: A Chemical Laser Simulation Computer Program," Technical Report H-CR-77-8, U.S. Army Missile Research and Development Command, February 1977.

18. von Mises, R., Mathematical Theory of Compressible Fluid Flow, Academic Press, 1958.

19. Oswatitsch, K., Gas Dynamics (English Version), Academic Press, 1956.

20. Courant, R. and Friedrichs, K. O., Supersonic Flow and Shock Waves, Interscience, 1948.

21. Benison, G. I. and Rubin, E. L., "A Time-Dependent Analysis for Quasi-One-Dimensional, Viscous Heat Conducting, Compressible Laval Nozzle Flows," J. of Eng. Math., Vol. 5, 1971, pp. 39-49.

22. Mitchell, A. R., Computational Methods in Partial Differential Equations, Wiley, 1969.

23. Kreiss, H. O., "Boundary Conditions for Difference Approximation of Hyperbolic Differential Equations," in AGARD Lecture Series No. 64; Advances in Numerical Fluid Dynamics, 1973, pp. 1-1, 1-13.

24. Ludford, G., Polachek, H., and Seeger, R. J., "On Unsteady Flow of Compressible Viscous Fluids," J. Appl. Phys., Vol. 24, 1953, pp. 490-495.

25. Moretti, G. and Salas, M. D., "Numerical Analysis of Viscous One-Dimensional Flows," in AGARD Lecture Series No. 48; Numerical Methods in Fluid Dynamics, 1972, pp. 7-1, 7-19.

UNCLASSIFIED
SECURITY CLASSIFICATION OF THIS PAGE (When Data Entered)

REPORT DOCUMENTATION PAGE	READ INSTRUCTIONS BEFORE COMPLETING FORM
1. REPORT NUMBER: AFOSR-TR-79-0085	2. GOVT ACCESSION NO. / 3. RECIPIENT'S CATALOG NUMBER
4. TITLE (and Subtitle): NUMERICAL MODEL DEVELOPMENT FOR LASER CAVITY FLOWFIELDS	5. TYPE OF REPORT & PERIOD COVERED: Interim, 31 May 77 - 31 May 78
	6. PERFORMING ORG. REPORT NUMBER: 9278-950001
7. AUTHOR(s): J.T. Schimke, W.L. Rushmore, and S.W. Zelazny	8. CONTRACT OR GRANT NUMBER(s): F49620-77-C-0076
9. PERFORMING ORGANIZATION NAME AND ADDRESS: Bell Aerospace Textron, Division of Textron, Inc., P.O. Box One, Buffalo, New York 14240	10. PROGRAM ELEMENT, PROJECT, TASK AREA & WORK UNIT NUMBERS: 61102F 2304/A3
11. CONTROLLING OFFICE NAME AND ADDRESS: Air Force Office of Scientific Research/NM, Bolling AFB, Washington, DC 20332	12. REPORT DATE: May 1978
	13. NUMBER OF PAGES: 68
14. MONITORING AGENCY NAME & ADDRESS (if different from Controlling Office): 70 p.	15. SECURITY CLASS. (of this report): UNCLASSIFIED
	15a. DECLASSIFICATION/DOWNGRADING SCHEDULE

16. DISTRIBUTION STATEMENT (of this Report)

Approved for public release; distribution unlimited.

17. DISTRIBUTION STATEMENT (of the abstract entered in Block 20, if different from Report)

18. SUPPLEMENTARY NOTES

19. KEY WORDS (Continue on reverse side if necessary and identify by block number)

Finite Elements
Sparse Matrix
Unsteady Flow
Laser Flow
Three-Dimensional Flow

20. ABSTRACT (Continue on reverse side if necessary and identify by block number)

A recently developed subroutine package for the integration of systems of ordinary differential equations by implicit methods is tested on a variety of gas dynamic problems. These problems include one-dimensional unsteady gas flow and two and three-dimensional parabolic (steady) Navier-Stokes problems. The governing partial differential equations were converted to systems of ordinary differential equations using either finite differences or finite elements, and then integrated by the implicit integration package. Included among the examples is a realistic steady laser cavity flow problem.

DD FORM 1 JAN 73 1473

408855

UNCLASSIFIED
SECURITY CLASSIFICATION OF THIS PAGE (When Data Entered)